DMD Fast Forward. Published on December 18, 2020 as DOI: 10.1124/dmd.120.000125
This article has not been copyedited and formatted. The final version may differ from this version.

Prediction of transporter-mediated drug-drug interactions and phenotyping of hepatobiliary transporters involved in the clearance of E7766, a novel macrocycle-bridged dinucleotide

Rongrong Jiang[*], Andrew Hart[1], Laurette Burgess, Dae-Shik Kim, Weidong Lai[2], Vaishali Dixit[*]

Drug Metabolism and Pharmacokinetics, Eisai Inc, Massachusetts, USA (R.J., V.D., G.L., A.H.)

Genetics Guided Dementia Discovery, Eisai Inc, Massachusetts, USA (L.B., DS.K.)

[1]*Current Address: Wave Life Sciences, Massachusetts, USA*

[2]*Current Address: Triplet Therapeutics, Massachusetts, USA*

[*]*Co-corresponding authors*

DMD Fast Forward. Published on December 18, 2020 as DOI: 10.1124/dmd.120.000125
This article has not been copyedited and formatted. The final version may differ from this version.

Running Title: Transporter-mediated drug-drug interactions for E7766

Co-corresponding authors

Dr. Rongrong Jiang, Drug Metabolism and Pharmacokinetics, Eisai Inc, Cambridge Massachusetts, USA. Tel: (857) 829-6063; E-mail: Rongrong_jiang@eisai.com

Dr. Vaishali Dixit, E-mail: dixitv77@gmail.com

Number of text pages: 25

Words in the Abstract: 243

Words in the Introduction: 591

Words in the Discussion: 1341

Number of references: 35

Number of Tables: 5

Number of Figures: 5

Number of Supplemental Tables: 4

Number of Supplemental Figures: 3

DMD Fast Forward. Published on December 18, 2020 as DOI: 10.1124/dmd.120.000125
This article has not been copyedited and formatted. The final version may differ from this version.

List of abbreviations

$A_{e\ fecal}$, amount excreted in feces; $A_{e\ biliary}$, amount excreted in bile; $A_{e\ renal}$, amount excreted in urine; BCRP, breast cancer resistance protein; BSEP, bile salt export pump; $CL_{biliary}$, hepatobiliary excretory clearance; CL_{fecal}, fecal excretory clearance; CL_{int}, intrinsic clearance; $CL_{tot,p}$, total plasma clearance; CL_{renal}, renal excretory clearance; K_m, Michaelis-Menten constant; MDR, multidrug resistance; MRP, multidrug resistance-associated protein; NCEs, new chemical entities; NTCP, Na^+/taurocholate cotransporting polypeptide; OAT, organic anion transporter; OATP, organic anion transporting polypeptide; OCT, organic cation transporter; PBPK, physiologically based pharmacokinetic; PK, pharmacokinetic; V_{max}, maximum transport velocity; V_{SS}, distribution volume at steady state.

DMD Fast Forward. Published on December 18, 2020 as DOI: 10.1124/dmd.120.000125
This article has not been copyedited and formatted. The final version may differ from this version.

Abstract

E7766 represents a novel class of macrocycle-bridged dinucleotides, and is under clinical development for immuno-oncology. In this report, we identified mechanism of systemic clearance E7766, investigated the hepatobiliary transporters involved in the disposition of E7766 and potential drug interactions of E7766 as a victim of organic anion transporting polypeptide (OATP) inhibitors. In bile-duct cannulated (BDC) rats and dogs, E7766 was mainly excreted unchanged in bile (>80%) and to a lesser extent in urine (<20%). Sandwich cultured human hepatocytes (SCHH), transfected cells and vesicles were used to phenotype the hepatobiliary transporters involved in the clearance of E7766. SCHH data showed temperature-dependent uptake of E7766, followed by active biliary secretion. In vitro transport assays using transfected cells and membrane vesicles confirmed that E7766 was a substrate of OATP1B1, OATP1B3 and multidrug resistance-associated protein 2 (MRP2). Phenotyping studies suggested predominant contribution of OATP1B3 over OATP1B1 in the hepatic uptake of E7766. Studies in OATP1B1/1B3 humanized mice showed that plasma exposure of E7766 increased 4.5-fold when coadministered with Rifampicin. Physiologically based pharmacokinetic (PBPK) models built upon two independent bottom-up approaches predicted elevation of E7766 plasma exposure when administered with Rifampicin, a clinical OATP inhibitor. In conclusion, we demonstrate that OATP-mediated hepatic uptake is the major contributor to the clearance of E7766 and inhibition of OATP1B may increase its systemic exposure. Predominant contribution of OATP1B3 in the hepatic uptake of E7766 was observed, suggesting polymorphisms in OATP1B1 would be unlikely to cause variability in the exposure of E7766.

DMD Fast Forward. Published on December 18, 2020 as DOI: 10.1124/dmd.120.000125
This article has not been copyedited and formatted. The final version may differ from this version.

Significance Statement

Understanding the clearance mechanisms of new chemical entities is critical to predicting human pharmacokinetics and drug interactions. A physiologically based pharmacokinetic model that incorporated parameters from mechanistic in vitro and in vivo experiments was used to predict pharmacokinetics and drug interactions of E7766, a novel dinucleotide drug. The findings highlighted here may shed a light on the pharmacokinetic profile and transporter-mediated drug interaction propensity of other dinucleotide drugs.

DMD Fast Forward. Published on December 18, 2020 as DOI: 10.1124/dmd.120.000125
This article has not been copyedited and formatted. The final version may differ from this version.

Introduction

Stimulator of interferon genes (STING) is an important innate immune sensor, and activation of STING plays a critical role in controlling cancer development by bridging the innate and adaptive immunities (Corrales et al., 2016; Woo et al., 2014). Significant efforts have been made by several pharmaceutical companies to develop potent agonists of the STING receptor (Marloyle et al., 2019). We have recently reported the discovery of E7766 (Figure 1), a potent STING agonist that belongs to a novel class of macrocycle-bridged dinucleotides (Endo et al., 2019). In nonclinical studies, E7766 has demonstrated potent antitumor activity by inducing a robust and effective innate and adaptive antitumoral immune response (Huang et al., 2019). Macrocycle-bridged dinucleotides were generally characterized by moderate to high molecular weight (>400), low logP (<1) and pKa of 3-4. Macrocycle-bridged dinucleotides also have low permeability, and as such fall in the Class 3B of the extended clearance classification system (ECCS) (Varma et al., 2015), thus making them potential substrates for hepatic uptake and efflux transporters. Many compounds in this series showed high clearance that was at or exceeded hepatic blood flow and had low volume of distribution. Additionally, the compounds were metabolically stable in rodent and human hepatocytes and liver S9 fraction indicating that metabolism was unlikely the primary clearance pathway. Identifying clearance mechanisms of these novel class compounds in drug discovery is important to predict systemic and target tissue exposure, as well as to predict clinical drug-drug interaction (DDI).

The significant clinical implications of inhibiting hepatic uptake transporters such as OATP1B have highlighted the importance of assessing this potential liability for new chemical entities (NCEs) during drug discovery and development (Chen et al., 2018). The US Food and Drug Administration (US FDA) and the European Medicines Agency (EMA) have also issued

DMD Fast Forward. Published on December 18, 2020 as DOI: 10.1124/dmd.120.000125
This article has not been copyedited and formatted. The final version may differ from this version.

guidance for the in vitro and in vivo evaluation of the transporter-based DDI (EMA, 2012; FDA, 2017). Predicting DDI for substrates of OATP1B1 and OAPT1B3 has recently been described in many reports (Duan et al., 2017; Yoshikado et al., 2018). Physiologically based pharmacokinetic (PBPK) modeling has been recognized to be a powerful tool for PK and DDI predictions of substrates of hepatic uptake transporters as well as drug metabolizing enzymes (Jones et al., 2015; Wang et al., 2017). In addition to predicting DDI, PBPK can also be used in the mechanistic understanding of various rate-limiting and rate-determining processes in the disposition of drugs.

E7766 was selected as a suitable model compound for investigating the clearance mechanisms and transporter-mediated DDI propensity of macrocycle-bridged dinucleotide-type STING agonists. A series of nonclinical studies were planned and conducted to 1) assess the major clearance mechanisms in the systemic clearance of E7766; 2) identify the transporters and estimate their relative contributions to the hepatic clearance of E7766, and 3) use the in vitro transporter data and PBPK model framework to prospectively predict the clinical DDI of E7766 with OATP1B inhibitor. To best of our knowledge, this is the first report for the identification of hepatobiliary transporters and PBPK modeling-based DDI prediction of therapeutically important and structurally novel macrocycle-bridged dinucleotides. Our data underscores the importance of OATP1B, especially OATP1B3, in determining the systemic hepatic clearance rate and hence the plasma exposure of E7766 and perhaps this class of compounds. Furthermore, our results also show that clinically relevant DDIs leading to changes in plasma exposure can occur if E7766 is coadministered with OATP1B3 inhibitors. The predominant contribution of OATP1B3 to the clearance of E7766 suggests that the plasma exposure to E7766 is less likely to be subjected to inter-individual variability due to polymorphisms in OATP1B1.

DMD Fast Forward. Published on December 18, 2020 as DOI: 10.1124/dmd.120.000125
This article has not been copyedited and formatted. The final version may differ from this version.

115

DMD Fast Forward. Published on December 18, 2020 as DOI: 10.1124/dmd.120.000125
This article has not been copyedited and formatted. The final version may differ from this version.

Materials and Methods

Chemicals and reagents

E7766 and the internal standard (IS), ER-001229535 (Lot No. ER-001229535-NH4-011), were synthesized at Eisai Inc. (Andover, MA). Bovine serum albumin solution was purchased from American Tissue Culture Collection (ATCC; Manassas, VA). Estradiol-17β-glucuronide ($E_2$17βG), Rifampicin, and Krebs-Henseleit buffer (KH buffer) were purchased from Sigma-Aldrich (St. Louis, MO). Porcine kidney LLC–PK1 (parentalcells were obtained from Discovery Labware, Inc (now Corning Inc., Tewkbury, MA). HEK293-FT cells stably transfected with the vector containing OATP1B1 cDNA or OATP1B3 cDNA, or empty vector were obtained from Solvo Biotechnology (Zeged, Hungary). TransportoCells™ transiently transfected with the vector containing OATP2B1 cDNA or NTCP cDNA, or empty vector were purchased from Corning (NY, USA). The cell culture related reagents were cell culture grade, and were purchased from Thermo Scientific, Inc. (Herndon, VA). All other reagents used in this study were of either analytical or HPLC grade.

Transport studies of E7766 with hepatic Solute Carrier (SLC) transporters

TransportoCells™ (Corning, NY, USA) transiently expressing OATP2B1 or NTCP and the control cells (HEK293 cells transfected with empty vector), and HEK293FT cell line (Solvo Biotechnology, Zeged, Hungary) stably expressing OATP1B1 (HEK293FT-OATP1B1) or OATP1B3 (HEK293FT-OATP1B3) and the control cells (HEK293FT-control; HEK293FT cells transfected with empty vector) were grown in a Dulbecoo's modified Eagle's medium fortified with 10% fetal calf serum and 2 mmol/L sodium butyrate (for NTCP only) in a humidified incubator at 37°C and 5% CO_2. Solvo HEK293-FT cells were harvested at 90% confluence and then seeded in poly-D-lysine-coated 24-well 24 h prior to transporter assay while Corning

DMD Fast Forward. Published on December 18, 2020 as DOI: 10.1124/dmd.120.000125
This article has not been copyedited and formatted. The final version may differ from this version.

TransportoCells™ were thawed and seeded in poly-D-lysine-coated 96-well 24 h prior to transporter assay. Cellular transport assays were conducted as described previously (Jiang et al., 2015). Briefly, cells were washed twice and pre-incubated with 200 μL of pre-warmed Krebs-Henseleit (KH) buffer. After pre-incubation, cells were incubated with 3 or 10 μmol/L of E7766 in presence or absence of 100 μmol/L of inhibitors (Rifamycin SV for OATP2B1, Troglitazone for NTCP, and Rifampicin for OATP1B1 and OATP1B3). The transport reaction was terminated by aspirating the buffer from the wells at designated time. After washing three times with 200 μL of ice-cold KH buffer, the cells were lysed and the resulting cellular lysates were analyzed by LC-MS/MS.

The time-dependent uptake of E7766 with OATP1B1 and OATP1B3 was evaluated to confirm linear uptake condition range of uptake of E7766 (Supplemental Figure 2). Concentration-dependent uptake of E7766 via OATP1B1 and OATP1B3 was examined with a concentration range of 0.25-100 μmol/L under linear conditions at 5 minutes. All experiments were run in triplicates.

Transport studies of E7766 with hepatic ABC transporters

TransportoCells™ membrane vesicles (Corning, NY, USA) expressing MDR1, BCRP, BSEP, or MRP2, and control vector vesicles (70 μL) were pre-incubated with vesicle uptake buffer (47 mmol/L MOPs-Tris, 65 mmol/L KCl, 7 mmol/L $MgCl_2$, pH 7.4 for MDR1 and BCRP; 47 mmol/L MOPs-Tris, 2.5 mmol/L GSH, 65 mmol/L KCl, 7 mmol/L $MgCl_2$, pH 7.4 for MRP2; and 10 mmol/L HEPES-Tris, 100 mmol/L KNO_3, 12.5 mmol/L $Mg(NO_3)_2$, and 50 mmol/L sucrose, pH 7.4 for BSEP) at 37 °C for 10 minutes. The transport was initiated by adding 125 μL of pre-warmed 25 mmol/L MgATP, 3 μmol/L of E7766 in the presence or absence of inhibitors (3 μmol/L of Novobioncin for BCRP, 100 μmol/L of MK-571 for MRP2, and 20 μmol/L of

DMD Fast Forward. Published on December 18, 2020 as DOI: 10.1124/dmd.120.000125
This article has not been copyedited and formatted. The final version may differ from this version.

Ketoconazole for MDR1 and BSEP). The transport was terminated at designated time by adding 200 μL ice-cold vesicle uptake buffer. The complete content was then rapidly filtrated using multi-screen HTS vacuum manifold, followed by 5 washes and filtrations. The plate was allowed to dry completely and then placed onto a 96-well receiver plate. A 50 μL of elute solution (75% methanol containing the internal standard) was added into each assay well followed by centrifugation at 2000 rpm for 5 minutes. This lysis-and-centrifugation procedure was repeated one more time to maximize compound extraction. The samples from two centrifugation were combined and analyzed by LC-MS/MS. All experiments were run in triplicates.

The LLC-PK1 cell-based permeability of E7766 was also assessed. Porcine kidney LLC-PK1 cells were cultured at 37 ºC and 5% CO2 in Medium 199 containing 10% fetal bovine serum, 292 μg/mL glutamine, 0.1 mg/mL hygromycin B, and 0.05 mg/mL gentamycin. The cells were seeded in HTS Transwell–96 systems (polystyrene, 4.26 mm in diameter, 0.14 cm^2 surface area, 1.0 μm in pore size, Corning Inc. Corning, NY) at a density of approximately 1.4×10^6 cells/mL. Culture medium was replaced on the fourth and sixth day after seeding. Cells were cultured for 7 days on Transwell plates for the studies. Prior to the experiments, LLC-PK1 cells were washed using transport buffer (HBSS supplemented with 10 mmol/L HEPES) and incubated for 60 minutes. For the experiments of apical to basolateral (A–B) direction, transport buffer containing 1 μmol/L of E7766 was added into the apical compartment while transport buffer with the same treatment was added into the basolateral compartment. For the experiments of basolateral to apical (B–A) direction, transport buffer containing 1 μmol/L of E7766 was added into the basolateral compartment while transport buffer with the same treatment was added into the apical compartment. The length of incubation for transport was 2 hours and samples were stored at –70 ºC or lower prior to LC-MS/MS analysis.

DMD Fast Forward. Published on December 18, 2020 as DOI: 10.1124/dmd.120.000125
This article has not been copyedited and formatted. The final version may differ from this version.

Hepatic uptake and biliary excretion of E7766 in sandwich cultured human hepatocytes (SCHH)

Transporter Certified™ cryopreserved human hepatocytes (BioIVT, Durham, NC, USA; Donor JEL) were thawed following manufacturer's instructions. Cryopreserved hepatocytes were subsequently suspended in BioIVT proprietary hepatocyte seeding medium (QualGro™ Seeding Medium) and seeded at a density of 0.9 million viable cells/mL onto BioCoat® 24-well cell culture plates (San Jose, CA, USA). Following plating, cells were allowed to attach for 2-4 hours, then were rinsed and fed with warm (37°C) seeding medium. Eighteen to 24 hours later, cells were fed and overlaid with QualGro™ culture medium (QTS, Durham, NC, USA) supplemented with extracellular matrix Matrigel® (BD Biosciences, San Jose, CA, USA; 0.25 $mg \cdot mL^{-1}$). Cells were then maintained in QualGro™ Hepatocyte Culture Medium. Hepatic uptake clearance and hepatobiliary disposition of test articles were assessed on day 5 by using B-CLEAR® Technology (Swift, Pfeifer & Brouwer, 2010). Briefly, to assess uptake clearance, cell culture medium was removed, and hepatocytes were washed three times with warm Plus (+) Buffer (0.3 mL per well). Immediately following washing step, dose solutions for E7766 or comparators (0.3 mL per well) were added and incubated for 1, 5, and 10 minutes at 37°C. Following incubation period, the solutions were collected and frozen at -80°C until process for bioanalysis. The wells were then washed three times with ice cold Plus (+) Buffer. The plates were frozen at -80 °C until bioanalysis.

To assess biliary clearance, cell culture medium was removed, and hepatocytes were washed twice with warm Plus (+) or Minus (-) Buffer to maintain or disrupt tight junctions, respectively. The wash solutions were removed and replaced with fresh Plus (+) Buffer or Minus (-) Buffer (0.3 mL per well). The hepatocytes were conditioned for 10 minutes at 37 °C.

DMD Fast Forward. Published on December 18, 2020 as DOI: 10.1124/dmd.120.000125
This article has not been copyedited and formatted. The final version may differ from this version.

The conditioning solutions were removed and replaced with dosing solutions for E7766 or comparators (0.3 mL per well). Following a 20-minute incubation, the solutions were collected and frozen at -80 ^{o}C until process for bioanalysis. The wells were then washed three times with ice cold Plus (+) Buffer. The plates were frozen at -80 °C until processed for bioanalysis. All experiments were run in triplicates.

In vivo Pharmacokinetics

All in vivo study protocols were approved by appropriate Institutional Animal Care and Use Committee. Animals were monitored during the study and provided free access to food and water.

Pharmacokinetics in bile-duct cannulated (BDC) rats and dogs

BDC male Sprague Dawley rats (n=4) and BDC male Beagle dogs (n=3) were given E7766 as a single 1 mg/kg IV dose and 0.075 mg/kg IV dose as free acid prepared in sterile PBS, respectively. Plasma samples were collected at pre-dose and designate time points post-dose via a jugular vein, into tubes containing sodium heparin as the anticoagulant. Urine samples were collected at intervals 0 to 4, 4 to 8, and 8 to 24 hours post-dose into collection tubes on wet ice. Bile and feces (rat only) samples were collected at intervals 0 to 4, 4 to 8, and 8 to 24 hours post-dose into collection tubes on wet ice. All samples were stored at –70 °C or lower until LC-MS/MS analysis.

Pharmacokinetics in humanized OATP1B1/1B3 and wild type (WT) mice

E7766 was formulated in 0.5% 0.1 N HCl, 5% DMSO, 10% EtOH, 84.5% saline for studies in WT and humanized OATP1B1/1B3 mice. Rifampicin was formulated in 0.5% 0.1 N HCl, 5% DMSO, 10% EtOH, 84.5% saline**.** Age-matched OATP1B1 and OATP1B3-knockin humanized

DMD Fast Forward. Published on December 18, 2020 as DOI: 10.1124/dmd.120.000125
This article has not been copyedited and formatted. The final version may differ from this version.

mice (n=3) on the Oatp1a/1b-knockout background, and wild-type (WT) FVB male mice (n=3/timepoint) were purchased from Taconic Biosciences (Hudson, NY, USA). Mice were between 8 and 10 weeks of age (22–34 g) at the time of study. In WT mice, E7766 was administered via the tail vein at a dose of 0.5 mg/kg with either vehicle or Rifampicin (30 mg/kg IV). Plasma and liver samples were collected at 0.083, 0.25, 0.5, 1, 1.5, 3, 6 hours and all samples were stored at -80°C until bioanalysis. In humanized mice, E7766 was administered via the tail vein at a dose of 1 mg/kg or together with vehicle or with Rifampicin (E7766, 0.5 mg/kg; Rifampicin, 10 mg/kg). Blood samples were collected at pre-dose, and 0.08, 0.25, 0.5 1, 1.5, 3, 6 and 24 hours post-dose via saphenous or tail vein into a heparinized capillary. The contents of the capillary were expelled onto an appropriate spot on a DBS card (FTA DMPK-B [GE Healthcare, Life Sciences, Whatman^{TM}]). Urine and feces samples were collected from all dose groups at intervals 0-8 and 8-24 hours post-dose. Samples were stored at -80°C until bioanalysis.

LC-MS/MS analysis

Cell lysates samples were extracted by 70:30 methanol:water (v:v) containing internal standard (IS) 10 nmol/L ER-001229535. Plasma samples were subjected to protein precipitation with methanol containing ER-001229535 as the IS. Urine, bile and feces samples were extracted via salting-out assisted liquid-liquid extraction based on the methodologies described by Tang and Weng, 2013. For analysis of E7766 and IS of ER-001229535, a Shimadzu HPLC system (Shimadzu Scientific Instruments, Columbia, MD), which consisted of an autosampler (model: SIL HTc), a column compartment unit (model: CTO-20AC), a degasser (model: DGU-20A3), two pumps (model: LC-20AD), and a high pressure switching valve (model: FCV-20AH6) was used. The mobile phase A consisted of 2 mmol/L ammonium bicarbonate in H_2O/MeOH (95/5, v/v), and mobile phase B consisted of 2 mmol/L ammonium bicarbonate in MeOH/H_2O (95/5,

v/v). Aliquots (10 μL) were injected onto a Waters XBridge Oligonucleotide BEH C18 column, 130Å, 2.5 μm (4.6 mm inner diameter × 50 mm length) at a flow rate of 0.5 mL/min at 40 °C. The temperature of the autosampler was controlled at 4 °C. The samples were analyzed on an API5000 (Sciex, Framingham, MA) triple quadrupole mass spectrometer with turbospray ionization (ESI) under negative ion mode. A 9 min gradient was run for E7766 and IS, with a flow rate of 0.5 mL/min as follows: 0% B for 0.3 min, 0% to 100% B over 2.7 min, 100% B for 2 min, 100% to 0% B over 0.2 min, then re-equilibration at 0% B for 3.8 min. Analytes were detected by multiple reaction monitoring (MRM) by the following mass transitions: 372.4 $(M-2H)^{2-}$ >186.5 for E7766 (-38 eV collisions) and 689.3 $(M-H)^{-}$ >134.1 for IS (-75 eV collisions).

PBPK model and DDI simulations

Whole-body PBPK modeling and simulation were performed using the population-based absorption, distribution, metabolism, and excretion simulator, Simcyp™ (version 18, Certara, Sheffield, UK). Each simulation was performed for 100 subjects (10 trials × 10 subjects) using the software's built-in healthy volunteer virtual population. To simulate the effect of OATP inhibitors on the PK of E7766, the PBPK model for Rifampicin-SD was adopted directly from the default Simcyp™ compound library. For all simulations, E7766 was administered as a single intravenous dose and Rifampicin was administered as a single oral dose. Physicochemical properties and input parameters for E7766 used for the PBPK model are summarized in Table 4. Parameters of Rifampicin for the DDI simulation are summarized in Supplemental Table 4

The full-PBPK model with Method 2 (based on Rodgers and Rowland) was used to predict the volume of distribution (V_d) of E7766 (Rodgers et al., 2005; Rodgers and Rowland, 2006). A K_p scalar of 4 was applied to the prediction of human V_d. The K_p scalar was determined based on the predicted versus observed V_d of E7766 in preclinical species. Permeability-limited

DMD Fast Forward. Published on December 18, 2020 as DOI: 10.1124/dmd.120.000125
This article has not been copyedited and formatted. The final version may differ from this version.

disposition was considered for liver. The DDI simulation was run in two scenarios: 1) Hepatic uptake clearance was assigned from the transporter kinetics (V_{max}/K_m) for OATP1B1 and OATP1B3 measured in the HEK293FT system, and intrinsic passive diffusion across the sinusoidal membrane measured in SCHH studies, and scenario 2) intrinsic active uptake clearance, passive clearance on the sinusoidal membrane and efflux clearance on the canalicular membrane, measured in the SCHH studies, were used to capture hepatobiliary disposition. In both scenarios, the intrinsic uptake clearances were scaled up to physiologically relevant uptake clearance by a relative expression factor (REF) approach (Hirano et al., 2004) within Simcyp models. Additionally, in second scenario, the intrinsic uptake clearance from SCHH was assigned to OATP1B3 (f_t =0.97) to capture the DDI. Based on in vitro metabolism data using cryopreserved human hepatocytes (data not shown), metabolic clearance was assumed to be negligible for both simulations. PK in preclinical studies suggest that E7766 is expected to be eliminated from kidney via glomerular filtration. The renal clearance of E7766 was then fixed as 3 L/h as a product of GFR (~6 L/h in human; Lin et al. 2003) and plasma protein binding of E7766 (0.5, measured data, Table 4). This fixed renal clearance also aligned well with back calculation from systemic clearance and the observation from PK studies of multiple preclinical species, where about 10% of E7766 was excreted in urine as parent compound. Sensitivity analysis was performed to evaluate changes in drug exposure and DDI due to any uncertainty in the in vitro parameters.

Data analysis

The uptake velocity describes the rate of E7766 taken up by active and/or passive processes of the transporter-expressing cell or vesicles, and is calculated as follows:

$$\text{uptake velocity} = (C \times V)/T/W \quad (1)$$

DMD Fast Forward. Published on December 18, 2020 as DOI: 10.1124/dmd.120.000125
This article has not been copyedited and formatted. The final version may differ from this version.

where C represents the concentration of E7766 in the cellular (or vesicular) lysate (μmol/L), V is the volume of the lysate (μL), T is the incubation time and W is the measured cellular (or vesicular) protein amount of each well (mg).

The OATP1B1 or OATP1B3 specific uptake velocity was calculated by subtracting mean uptake velocity of E7766 in HEK293-Control cells from that of HEK293FT-OATP1B1 or HEK293FT-OATP1B3 cells at each of the corresponding concentration. Kinetic and statistical analyses of the transport data were conducted using GraphPad Prism Ver. 7.02 (GraphPad Software, Inc., San Diego, CA). Kinetic data was fit to a Michaelis-Menten model as follows:

$$v = V_{max} \times S/[K_m + S] \quad (2)$$

where v is the OATP1B1 or OATP1B3 specific uptake velocity (pmol/mL/mg protein), S is the concentration of E7766 in the uptake buffer (μmol/L), K_m is the apparent Michaelis-Menten constant (μmol/L), and V_{max} is the apparent maximum uptake rate (pmol/min/mg protein). The in vitro intrinsic clearance ($CL_{int,in\ vitro}$) was calculated as follows:

$$CL_{int,in\ vitro} = V_{max}/K_m \quad (3)$$

The relative contribution of OATP1B1 and OATP1B3 to the hepatic uptake of E7766 was assessed by the relative expression factor (REF) approach (Kunze et al., 2014). REF for each transporter was calculated by following equations:

$$REF_{1B1} = EXP_{OATP1B1,HEP}/EXP_{OATP1B1,HEK} \quad (4)$$

$$REF_{1B3} = EXP_{OATP1B3,HEP}/EXP_{OATP1B3,HEK} \quad (5)$$

where EXP represents the specific transporter expression (fmol/mg protein) determined in primary human hepatocyte (HEP), or HEK293FT-OATP1B1 or HEK293FT-OATP1B3 cell line

DMD Fast Forward. Published on December 18, 2020 as DOI: 10.1124/dmd.120.000125
This article has not been copyedited and formatted. The final version may differ from this version.

(HEK). The expression levels of OAPT1B1 and OATP1B3 in hepatocyte and HEK293-FT overexpressing cell line are summarized in Supplemental Table 2.

For SCHH assays, the intrinsic hepatic uptake clearance (Liver Uptake $CL_{int,T}$) was determined using following:

$$\text{Uptake } CL_{int,T} = A_{\text{Plus (+)Buffer}} / (T \times C_{\text{initial}}) \quad (6)$$

where $A_{\text{Plus (+)Buffer}}$ is the total accumulation of E7766 (cells + bile pocket) in SCHH after incubation with Plus (+) buffer (μmol), T is the incubation time (min), and C_{initial} is the initial concentration of E7766 in dosing medium (μmol/L).

The biliary excretion index (BEI) was obtained from equation 7 and intrinsic biliary clearance (Liver Efflux $CL_{int,T}$) was calculated from equation 8:

$$\text{BEI} = 100 \times [A_{\text{Plus (+)Buffer}} - A_{\text{Minus(-)Buffer}}]/A_{\text{Plus (+)Buffer}} \quad (7)$$

$$\text{Efflux } CL_{int,T} = [A_{\text{Plus (+)Buffer}} - A_{\text{Minus(-)Buffer}}]/ (T \times C_{\text{initial}}) \quad (8)$$

where $A_{\text{Minus(-)Buffer}}$ is cellular accumulation inside hepatocytes (cells only) after incubation with Minus (−) buffer (μmol).

PK parameters of E7766 were obtained by non-compartmental analysis using Phoenix WinNonlin® Ver. 7.0.0.2535 (Certara USA, Inc., Princeton, NJ, USA). The parameters calculated were the cumulative amount of E7766 recovered in urine ($Xu_{(0\text{-}t)}$), bile ($Xb_{(0\text{-}t)}$) and feces ($Xf_{(0\text{-}t)}$), which were determined as the sum of the amounts recovered in each sampling interval; the percent of the administered dose excreted in urine ($A_{e\ renal}$ %), bile ($A_{e\ biliary}$ %) and feces ($A_{e\ fecal}$ %); and the renal (CL_{renal}), biliary ($CL_{biliary}$) and fecal clearances (CL_{fecal}), which were calculated using the cumulative amount recovered up to the last measurable urine, bile, or feces sample along with the $AUC_{(0\text{-}t,\ last)}$ as $CL_{renal} = Xu_{(0\text{-}t,\ last)} / AUC_{(0\text{-}t,\ last)}$ / body weight,

DMD Fast Forward. Published on December 18, 2020 as DOI: 10.1124/dmd.120.000125
This article has not been copyedited and formatted. The final version may differ from this version.

345 $CL_{biliary} = Xb_{(0\text{-}t,\ last)} / AUC_{(0\text{-}t,\ last)}$ / body weight and $CL_{fecal} = Xf_{(0\text{-}t,\ last)} / AUC_{(0\text{-}t,\ last)}$ / body

346 weight, respectively.

347

DMD Fast Forward. Published on December 18, 2020 as DOI: 10.1124/dmd.120.000125
This article has not been copyedited and formatted. The final version may differ from this version.

Results

Assessment of E7766 as a substrate of hepatic uptake transporters

As shown in Figure 2A, OATP1B1 and OATP1B3 showed significant active uptake of E7766 (p<0.000001 and p=0.000021 for OATP1B1 and OATP1B3, respectively), which could be inhibited by Rifampicin (100 µmol/L; p<0.000001 and p=0.000007 for OATP1B1 and OATP1B3, respectively). Active uptake of E7766 was not observed in cells expressing OATP2B1 (p=0.11) or NTCP (p=0.11). The results indicated that E7766 is a substrate for OATP1B1 and OATP1B3 but not a substrate for OATP2B1 and NTCP. We observed differences in passive uptake of E7766 with mock cells groups and this was at least partially due to the differences in cell subtypes, cell engineering, culture conditions and assay conditions. Additionally, very low passive permeability of E7766 could add further variability of passive uptake with mock cells. To support the validation of in vitro assay systems, uptake activity of positive control substrates was summarized in Supplemental Figure 1A.

The results of concentration-dependent uptake of E7766 in HEK293FT-OATP1B1, HEK293FT-OATP1B3, and HEK293FT-Control cells are summarized in Figure 3. The data were best-fitted to a Michaelis-Menten model, and the kinetic parameters for uptake of E7766 by OATP1B1 were calculated as 2.2 µmol/L (K_m) and 27.8 pmol/min/mg protein (V_{max}). The in vitro uptake clearance ($CL_{int,in\ vitro}$) of OATP1B1 was then calculated to be 12.6 µL/min/mg protein. The K_m, V_{max}, and $CL_{int,in\ vitro}$ of OATP1B3-mediated uptake of E7766 were estimated as 4.0 µmol/L, 81.3 pmol/min/mg protein, and 20.5 µL/min/mg protein, respectively. The relative expression factors (REFs) for OATP1B1 and OATP1B3 were calculated to be 0.1 and 2.8, respectively using the measured expression of these transporters in the overexpressing cell lines and the reported expression levels in human hepatocytes from Schaefer et.al, 2012

DMD Fast Forward. Published on December 18, 2020 as DOI: 10.1124/dmd.120.000125
This article has not been copyedited and formatted. The final version may differ from this version.

(Supplemental Table 2). We decided to use the transporter expression reported by Schaefer et.al, 2012 because the methodology used to extract the membrane protein and measure the protein content aligned with the methodology used to measure transporter expression in our HEK293FT overexpressing system.

Assessment of E7766 as a substrate of biliary efflux transporters

E7766 was incubated with either MDR1, BCRP, BSEP or MRP2 expressing or control vesicle membranes. As shown in Figure 2B, E7766 did not show transporter-mediated uptake activities in MDR1 (p>0.99), BCRP (p=0.17) and BSEP (p=0.45) expressing vesicles. Incubation of E7766 with MRP2-expressing vesicles resulted in greater uptake activity than that with control vesicles with an uptake ratio of 23 and a p-value of 0.00014. Co-incubation of E7766 and positive control inhibitor MK-571 (100 µmol/L) with MRP2 expressing vesicles, decreased the uptake ratio from 23 to 1.1 (p=0.00014). The results indicated that E7766 is a substrate of efflux transporter MRP2, but not a substrate of MDR1, BCRP or BSEP (Figure 2B). The transporter activity of positive control substrates for MDR1, MRP2, BCRP and BSEP is shown in Supplemental Figure 1B. The transcellular permeability of E7766 was assessed in LLC-PK1 cells. The results, as shown in Supplemental Table 1 indicated that E7766 exhibited very low permeability in LLC-PK1 cells (P_{app}<1×10^{-6} cm/s).

Evaluation of hepatic uptake and biliary excretion of E7766 in SCHH

The transporter-mediated hepatic uptake potential of E7766 was evaluated in SCHH prepared from one donor (JEL). The intrinsic hepatic uptake clearance of E7766 (uptake $CL_{int,T}$) at 4 ºC was markedly decreased to <7.6% of that at 37 ºC at two lower dose levels (0.3 and 1.0 µmol/L) (Table 1). The uptake $CL_{int,T}$ of E7766 across all dose levels dropped rapidly from 1 to 5 minutes (Table 1). These results suggested hepatic uptake was rapidly achieving near maximal

DMD Fast Forward. Published on December 18, 2020 as DOI: 10.1124/dmd.120.000125
This article has not been copyedited and formatted. The final version may differ from this version.

accumulation within 5 minutes. In addition, the uptake $CL_{int,T}$ decreased dramatically at 10 μmol/L across all exposure periods compared to uptake $CL_{int,T}$ measured at 0.1 μmol/L and 3 μmol/L suggesting hepatic uptake was saturated at concentration of >1.0 μmol/L (Table 1). Taken together, these results suggested that hepatic uptake of E7766 was primarily mediated by a relatively fast active uptake mechanism.

As shown in Table 1, following 20-minute exposure, the intrinsic biliary efflux clearance (efflux $CL_{int,T}$) decreased dramatically at 10 μmol/L compared to those at doses of 0.3 and 1 μmol/L suggesting hepatobiliary transport of E7766 was saturated at concentration of >1.0 μmol/L. The BEI of E7766 ranged from 70.9 to 86.2% across the concentration range assessed. These BEI values were comparable to d8-TCA (72.6%), a model bile acid, and was ~2-fold greater than the reference compound rosuvastatin (BEI = 42.7%). The difference in BEI for Rosuvastatin and d8-TCA/E7766 are likely due to differences in uptake and efflux mechanisms as well as kinetics of uptake and efflux of these compounds in the SCHH system. Overall, these results suggested the biliary excretion of E7766 is mediated by a saturable mechanism and with a relatively high BEI value.

Pharmacokinetics of E7766 in bile-duct cannulated BDC rats and dogs

The PK of E7766 in BDC rats (Table 2) was characterized by high $CL_{tot.p}$ (6.50 L/h/kg) and moderate V_{ss} (2.47 L/kg). The mean $Xu_{(0-t)}$ and $Xb_{(0-t)}$ up to 24 hours postdose were 38,600 and 261,000 ng, respectively, which corresponds to 13.7% ($A_{e\ renal}$) and 92.1% ($A_{e\ biliary}$) of the total dose administered, respectively. The mean cumulative amount of E7766 excreted in feces ($Xf_{(0-t)}$) up to 24 hours postdose was 991 ng, which correspond to 0.4% of the total dose administered ($A_{e\ fecal}$). Mean CL_{renal}, $CL_{biliary}$ and CL_{fecal} of E7766 in BDC rats were 0.895 L/h/kg, 6.04 L/h/kg and 0.0227 L/h/kg, respectively.

DMD Fast Forward. Published on December 18, 2020 as DOI: 10.1124/dmd.120.000125
This article has not been copyedited and formatted. The final version may differ from this version.

The PK of E7766 in BDC dogs (Table 2) was characterized by moderate total plasma clearance ($CL_{tot.p}$, 1.29 L/h/kg) and limited volume of distribution (V_{ss}, 0.553 L/kg). The mean cumulative amounts of unchanged E7766 excreted in urine ($Xu_{(0-t)}$) and bile ($Xb_{(0-t)}$) up to 48 hours postdose were 33,400 and 625,000 ng, respectively, which correspond to 5.0% ($A_{e\ renal}$) and 87.9% ($A_{e\ biliary}$) of the total dose administered, respectively. Mean renal (CL_{renal}) and biliary ($CL_{biliary}$) clearances of E7766 in dogs were 0.0528 L/h/kg and 1.19 L/h/kg, respectively.

Pharmacokinetics of E7766 in OATP1B1/1B3 humanized and wild type (WT) mice

The plasma and liver PK of E7766 in WT mice was assessed with or without coadministration of Rifampicin (Figure 4). The unbound concentration-time profiles of Rifampin in wild type and humanized mice are shown in Supplemental Figure 3. The plasma PK of E7766 in WT was characterized by high $CL_{tot.p}$ (8.93 L/h/kg) and moderate V_{ss} (1.66 L/kg) (Table 3). In the presence of Rifampicin, the plasma exposure (AUC_{total}) of E7766 in WT mice increased 5.4-fold with a corresponding decrease in $CL_{tot.p}$. The liver exposure to E7766 was comparable in WT mice with or without coadministration of Rifampicin indicating that Rifampicin only affects the plasma exposure and that liver exposure is unchanged by Rifampicin. However, the liver-to-plasma ratio $K_{p,total}$ of E7766 in Rifampicin treated animals decreased by 82% indicating a strong inhibition of Oatp mediated hepatic uptake of E7766 in mice (Table 3). The dose normalized plasma exposure (AUC_{total}/Dose) and $CL_{tot.p}$ were compared between WT mice (AUC_{total}/Dose: 112 ng/h/mL^{-1}/[mg/kg] and $CL_{tot.p}$: 8.93 L/h/kg) and OATP1B1/1B3 humanized mice (AUC_{total}/Dose: 126 ng/h/mL^{-1}/[mg/kg] and $CL_{tot.p}$: 9.20 L/h/kg). The dose normalized AUC in humanized mice increased 4.8-fold after coadministration with Rifampicin, which aligned with the increase in AUC (5.4-fold) in WT mice. We also assessed the percentage of the E7766 dose excreted in the urine and feces in the above studies (Figure 4). The dose excreted in the feces in

DMD Fast Forward. Published on December 18, 2020 as DOI: 10.1124/dmd.120.000125
This article has not been copyedited and formatted. The final version may differ from this version.

both WT and OATP1B1/1B3 humanized mice decreased to a similar extent (3-fold lower in WT mice and 4.6-fold lower in humanized mice) in the presence of Rifampicin. This decrease is in line with the corresponding increase in systemic exposure to E7766 in the presence of Rifampicin.

PBPK modeling and DDI simulation of E7766

The predicted plasma PK and systemic clearance as well as AUC ratio of E7766 in the presence and absence of Rifampicin are presented in Figure 5 and Table 5. In scenario one of the DDI simulation, active uptake clearances measured as J_{max}/K_m in HEK293 cells were assigned to OATP1B1 and OATP1B3, and the passive sinusoidal and biliary efflux clearances were taken from the SCHH experiment. Based on the REF factor and the in vitro uptake kinetics, the f_t for OATP1B3 and OATP1B1 were predicted to be 0.97 and 0.02, respectively, thus suggesting that OATP1B3 plays a predominant role in the hepatic uptake of E7766 (Figure 5A). The contribution of passive sinusoidal diffusion clearance to the overall uptake CL of E7766 was negligible (1%, Figure 5A). This simulation showed that the plasma AUC_{total} increases by 2.77-fold whereas the C_{max} in the presence of Rifampicin is unchanged (Figure 5B). The free liver intracellular C_{max} of E7766 in the presence of Rifampicin decreases by 31.1% and E7766 concentration further decreases to 72.6% at 1 hour after dosing due to impairment of OATP1B function. However, as shown in Figure 5C after 1 hour, the liver intracellular concentration starts to increase at later time points and therefore results in an unchanged liver intracellular AUC_{free} (69.06 nmoL/h/L, Table 5) in presence of Rifampicin compared to Rifampicin free group (76.19 nmoL/h/L, Table 5). This increase of liver concentrations at later time points is due an increase in the systemic exposure of E7766 in the presence of Rifampicin. A sensitivity analysis was performed for the in vitro parameters with uncertainty. As shown in Figure 5D-F, the change in

AUC ratio ranged from 1.0 to 2.6 when the REF or kinetic parameters for OATP1B3 were varied. The AUC ratio remained unchanged when the REF or kinetic parameters for OATP1B1 was varied indicating that the DDI was not sensitive to changes in J_{max}, K_m and REF for OATP1B1. It is noteworthy that, AUC ratio first increases along with the increase of OATP1B3 REF (when OATP1B3 REF< 3) and then starts to drop as OATP1B3 REF increased further until AUC ratio becomes ultimately close to unity (Figure 5D). One potential reason for this pattern maybe that, the hepatic uptake clearance increases when the OATP1B3 REF increased and will result in a larger DDI magnitude, i.e., a greater AUCR in the beginning when REF is in a relatively low range. However, as the OATP1B3 REF increases further (above three), the intrinsic uptake clearance will exceed hepatic blood flow and become a blood-flow rate limited process. Therefore the AUC is not readily affected by inhibition of uptake clearance. We speculate that another explanation may be that E7766 is being cleared away from the transporter binding site very rapidly when REF increases further. Thus there is not enough duration of exposure for E7766 (given as i.v. bolus dose) to have interaction with orally administered Rifampicin, which needs time to get to the interaction site in liver.

In the second scenario, DDI was simulated using active uptake, passive sinusoidal uptake and biliary efflux clearances measured in SCHH experiment. In this simulation, we observed similar results for both PK profile and DDI potential of E7766 as victim compared to the first scenario. The comparison between two different scenarios are summarized in Table 5. Simulation showed that the plasma AUC increases by 2.59-fold whereas the C_{max} in the presence of Rifampicin is unchanged. The liver AUC_{free} calculated by free intracellular concentrations remained unchanged in the presence of Rifampicin with a liver AUC_{free} ratio of 0.86. The

485 consistency of prediction from two scenarios which adopted experimental data from two
486 independent approaches suggests that the PBPK model is mechanistically sound.
487

DMD Fast Forward. Published on December 18, 2020 as DOI: 10.1124/dmd.120.000125
This article has not been copyedited and formatted. The final version may differ from this version.

Discussion

E7766 is a macrocycle-bridged dinucleotide under development as an immuno-oncology drug to be used as a single agent or in combination with other standard of care therapies. For several drugs such as pravastatin which are cleared primarily via biliary excretion, hepatic uptake is in fact the rate limiting step (Nakai et al., 2001), and inhibition of these uptake processes or polymorphisms in the hepatic uptake transporters may lead to clinically relevant change in the PK of drugs (Chen et al., 2018). Therefore, in vitro and in vivo studies were conducted for E7766 to systemically investigate drug transporters involved in its systemic clearance and to predict clinical DDI potential using PBPK models.

PK and excretion studies of E7766 were first conducted using BDC rats and BDC dogs. The results confirmed that biliary excretion plays predominant role in systemic clearance of E7766. To further study the clearance mechanisms of E7766, DDI studies with Rifampicin were conducted with OATP1B1/1B3 humanized and WT mice. Coadministration with Rifampicin in OATP1B1/1B3 humanized mice as well as WT mice resulted in an approximately 5-fold decrease in plasma clearance of E7766. We also measured the liver exposure of E7766 with and without coadministration with Rifampicin in WT mice. While liver AUC was comparable between mice with or without Rifampicin, the observed decrease in liver/plasma ratio (liver $K_{p,total}$) in WT mice in the presence of Rifampicin is consistent with hepatic OATP-mediated uptake. Studies in bile-duct cannulated dogs and rats show that biliary excretion of unchanged drug is the major route of clearance in preclinical species. Fecal excretion of unchanged drug was also observed in humanized and WT animals and excretion into the feces decreased substantially in animals where liver OATP/oatp function was inhibited. Taken together these results suggest that E7766 is cleared from systemic circulation primarily via active uptake into

DMD Fast Forward. Published on December 18, 2020 as DOI: 10.1124/dmd.120.000125
This article has not been copyedited and formatted. The final version may differ from this version.

the liver by OATP/oatp and then excreted unchanged into the bile. Previous reports have shown that hepatic expression of OATP1B1 in the humanized mice was lower than in human liver whereas the expression of OATP1B3 was 3-fold higher than in human liver (Higgins et al., 2014). These differences in the expression could lead to the overestimation of the contribution of OATP1B3 on the systemic exposure of OATP substrates in humanized mice. However, OATP1B1/1B3 humanized mice may still be useful in qualitatively determining whether hepatic OATP can impact systemic exposure and hepatic distribution of substrates.

To prospectively predict clinical DDI potential for E7766 as the victim drug, we used in vitro kinetic data generated from transporter overexpressing cell lines coupled with REF approach (scenario one) and Cl_{int} data from SCHH coupled with REF approach (scenario two) to build "bottom-up" full PBPK models and run DDI simulations. DDI simulation with Rifampicin suggests that Rifampicin may cause about 2-3 fold increase in plasma AUC in both scenarios, indicating that the current PBPK model is mechanistically sound. Similar to the findings in mice treated with Rifampicin, PBPK simulation showed that the intracellular free liver AUC did not change with treatment with Rifampicin, however the liver-to-plasma ratio decreased in the presence of Rifampicin. Previously reported PBPK approaches suggested the need for empirical scaling factors for hepatic active uptake to recover human PK of several OATP substrates (Jones et al., 2012; Watanabe, et al.,2009). These scaling factors are derived from "top down" approaches and are often compound specific (Varma et al., 2013). Hence the model developed here will need to be verified and E7766 specific scaling factors will be derived once clinical PK and DDI data for E7766 are available.

For prospective DDI assessment, a sensitivity analysis of parameters that have high uncertainty is important. For transporter-mediated DDIs, there is significant uncertainty due to

DMD Fast Forward. Published on December 18, 2020 as DOI: 10.1124/dmd.120.000125
This article has not been copyedited and formatted. The final version may differ from this version.

the limited understanding of quantitative translation of in vitro transporter kinetics to the clinical scenario. Hence we conducted a sensitivity analysis of the in vitro J_{max}, K_m and REF values. The sensitivity analysis results showed that AUC ratio is less sensitive to changes in the kinetic parameters for OATP1B1 than those of OATP1B3 due to predominant role of OATP1B3 in the overall clearance. On the other hand, based on f_t of E7766 for OATP1B1 and the sensitivity analysis, we can conclude that the pharmacokinetics of E7766 is less likely to be influenced by polymorphisms in OATP1B1. While the impact of genetic polymorphisms of OATP1B1 on the PK/PD of OATP1B substrates has been well documented (Niemi et al., 2011), that of OATP1B3 polymorphisms has not been clearly reported. Reduced uptake of glibenclimide and glipizide by OATP1B3 in HEK cells expressing OATP1B3 (699G > A) was recently reported (Yang et al, 2018). However, there are no reported clinical studies to support these in vitro observations. It is however advisable to genotype patients and healthy volunteers for any potential OATP1B3 polymorphisms to understand any inter-individual variability in E7766 exposure.

E7766 was also identified as a novel substrate of MRP2, an efflux transporter expressed on the canalicular membrane of human hepatocytes. MRP2 is essential for hepatobiliary and renal elimination of many anionic substrates, including drugs and conjugates such as bilirubin glucuronides (Nies and Keppler, 2007). It was reported that Rifampicin when dosed 600 mg orally may inhibit MRP2-mediated biliary excretion of (15R)-^{11}C-TIC-Me (Takashima et al., 2012). However, it is likely that the OATP mediated uptake rather than MRP2 mediated efflux influences the systemic exposure of E7766. This conclusion is based on, 1) ECCS classification which states that hepatic uptake will be the major contributor to the clearance of class 3B compounds and, 2) Others reported (Watanabe, et al., 2009) that the impairment of MRP2 would only affect the liver AUC but has no impact on plasma AUC if the compound is uptake limited.

To the best of our knowledge, no systemic DDI has been attributed to MRP2, and there is no evidence that MRP3 or MRP4 should be examined or that there is a likelihood of DDI for a substrate of MRP2 (Hillgren et al., 2013).

Further studies are warranted to investigate whether other dinucleotide NCEs are also substrates of OATP1Bs and MRP2. A recent paper published by Luteijn and coworkers (Luteijn et al., 2019) identified SLC19A1 (folate–organic phosphate antiporter) as the major transporter to facilitate cellular uptake of cyclic dinucleotides such as 2'3'-cGAMP into THP-1 cells and therefore has implications for the immunotherapeutic treatment of cancer. The uptake of 2'3'-cGAMP was inhibited by methotrexate and sulfasalazine, inhibitors of SLC transporters. OATP1B1, OATP1B3 and other OATP transporters are also found in multiple cancer cells including breast cancer, colon cancer, liver cancer, pancreatic cancer, prostate cancer, testicular cancer, and thyroid cancer (Pressler et al., 2011; Wlcek et al., 2008). Given that cellular permeability of E7766 or its analogs could be low due to their physiochemical properties, additional investigation into whether other analogs of E7766 are substrates of OATP1B1/1B3, SLC19A1 or other OATP transporters expressed in hepatocytes, immune cells or cancer cells can provide insight into ADME properties and pharmacological function of these novel NCEs.

In summary, our data show that transporter-mediated hepatic uptake is the major contributor to the overall systemic clearance of E7766. Based on the estimated f_t for OATP1B3 and OATP1B1 we conclude that OATP1B3 plays a predominant role in the hepatic uptake of E7766. The findings reported here have a significant influence on the design of clinical pharmacology program for E7766. Due to near complete recovery of unchanged E7766 observed in preclinical animal studies, the clinical protocols emphasized the need for collecting urine and fecal samples from patient volunteers in Phase I studies to measure the recovery of E7766 in

early clinical studies, which will give us useful information about renal and biliary clearances of E7766 in humans. This information could help design an appropriate human ADME study and accelerate clinical development of E7766. Since nonclinical studies have identified transporters responsible for clearance of E7766, appropriate clinical DDI studies can be designed and the PBPK model developed here can be used to predict DDI with perpetrators or co-administered therapies. Finally, the results collected from current studies may also shed light on pharmacokinetics and pharmacodynamics of other compounds from this class of macrocycle-bridged dinucleotides.

DMD Fast Forward. Published on December 18, 2020 as DOI: 10.1124/dmd.120.000125
This article has not been copyedited and formatted. The final version may differ from this version.

Acknowledgements

The authors would like to thank Kazutomi Kusano, Takafumi Komori, Yoshitane Nozaki, Naomi Wakayama, Saki Izumi and Raku Shinkyo from Eisai Co. LTD., Tsukuba, Japan for review and helpful scientific discussions during the preparation of this manuscript.

DMD Fast Forward. Published on December 18, 2020 as DOI: 10.1124/dmd.120.000125
This article has not been copyedited and formatted. The final version may differ from this version.

Authorship Contributions

Participated in research design: Jiang, Dixit, Hart, Lai

Conducted Experiments: Jiang, Hart, Burgess

Contributed new reagents or analytic tools: Kim

Performed Data analysis: Jiang, Dixit, Hart

Wrote or contributed to the writing of the manuscript: Jiang, Dixit

References

Chen Y, Zhu R, Ma F, Mao J, Chen EC, Choo EF Sahasranaman S and Liu L (2018) Assessment of OATP transporter-mediated drug-drug interaction using physiologically-based pharmacokinetic (PBPK) modeling - a case example. *Biopharm Drug Dispos* 39: 420-430.

Corrales L, McWhirter SM, Dubensky TW, Jr. and Gajewski TF (2016) The host STING pathway at the interface of cancer and immunity. *J Clin Invest* 126: 2404-2411.

Duan P, Zhao P and Zhang L (2017) Physiologically Based Pharmacokinetic (PBPK) Modeling of Pitavastatin and Atorvastatin to Predict Drug-Drug Interactions (DDIs). *Eur J Drug Metab Pharmacokinet* 42: 689-705.

EMA (2012) Guideline on the investigation of drug interactions.

Endo A, Kim DS, Huang KC, Hao M, Mathieu S, Choi HW, Majumder U, Zhu X, Shen Y, Sanders K, Noland T, Chandra D, Chen Y, Tendyke K, Loiacono K, Kolber-Simonds D, Jiang R, Dixit V, Hutz J, Wang J, Bao X, Fang F and Sarwar N (2019) Discovery of E7766: A representative of a novel class of macrocycle-bridged STING agonists (MBSAs) with superior potency and pan-genotypic activity. *Cancer Res* 79: Abstract nr 4456.

FDA (2017) In Vitro Metabolism- and Transporter- Mediated Drug-Drug Interaction Studies Guidance for Industry

Higgins JW, Bao JQ, Ke AB, Manro JR, Fallon JK, Smith PC and Zamek-Gliszczynski MJ(2014) Utility of Oatp1a/1b-knockout and OATP1B1/3-humanized mice in the study of OATP-mediated pharmacokinetics and tissue distribution: case studies with pravastatin, atorvastatin, simvastatin, and carboxydichlorofluorescein. *Drug Metab Dispos* 42: 182-192.

Hillgren KM, Keppler D, Zur AA, Giacomini KM, Stieger B, Cass CE, Zhang L and International Transporter Consortium (2013) Emerging transporters of clinical importance: an update from the International Transporter Consortium. *Clin Pharmacol Ther* 94: 52-63.

623 Hirano M, Maeda K, Shitara Y and Sugiyama Y (2004) Contribution of OATP2 (OATP1B1) and OATP8
624 (OATP1B3) to the hepatic uptake of pitavastatin in humans. *J Pharmacol Exp Ther* 311:139-146.
625 Jiang R, Dong J, Li X, Du F, Jia W, Xu F, Wang F, Yang J, Niu W and Li C (2015) Molecular
626 mechanisms governing different pharmacokinetics of ginsenosides and potential for ginsenoside-
627 perpetrated herb-drug interactions on OATP1B3. *Br J Pharmacol* 172: 1059-1073.
628 Jones HM, Barton HA, Lai Y, Bi YA, Kimoto E, Kempshall S, Tate SC, EI-Kattan A, Houston JB,
629 Galetin A and Fenner KS (2012) Mechanistic pharmacokinetic modeling for the prediction of transporter-
630 mediated disposition in humans from sandwich culture human hepatocyte data. *Drug Metab Dispos* 40:
631 1007-1017.
632 Jones HM, Chen Y, Gibson C, Heimbach T, Parrott N, Peters SA, Snoeys J, Upreti VV, Zheng M and
633 Hall SD (2015) Physiologically based pharmacokinetic modeling in drug discovery and development: a
634 pharmaceutical industry perspective. *Clin Pharmacol Ther* 97: 247-262.
635 Huang KC, McGrath S, Chandra D, Wu J, Kim DS, Albu D, Ingersoll C, Tendyke K, Loiacono K,
636 Noland T, Verbel D, Zhang C, Hao MH, Matijevic M, Dixit V, Hukkanen RR, Hutz J, Wang J, Fang F,
637 Bao X, Kolber-Simonds D, Akram M and Sarwar N.(2019) Discovery and characterization of E7766, a
638 novel macrocycle-bridged STING agonist with pan-genotypic and potent antitumor activity through
639 intravesical and intratumoral administration. *Cancer Res* 79: Abstract nr 3269.
640 Kunze A, Huwyler J, Camenisch G and Poller B (2014) Prediction of organic anion-transporting
641 polypeptide 1B1- and 1B3-mediated hepatic uptake of statins based on transporter protein expression and
642 activity data. *Drug Metab Dispos* 42: 1514-1521.
643 Lin J, Knight EL, Hogan ML and Singh AK (2003). A comparison of prediction equations for estimating
644 glomerular filtration rate in adults without kidney disease. *J Am Soc Nephrol* 14: 2573-2580.
645 Luteijn RD, Zaver SA, Gowen BG, Wyman SK, Garelis NE, Onia L, McWhirter SM, Katibah GE, Corn
646 JE, Woodward JJ and Raulet DH (2019). SLC19A1 transports immunoreactive cyclic dinucleotides.
647 *Nature* 573: 434-438.

Marloyle M, Lawler SE, Berger G (2019) Current patent and clinical status ofstimulator of interferon genes (STING) agonists for cancer immunotherapy. *Pharm. Pat. Anal* 8: 87-90

Nakai D, Nakagomi R, Furuta Y, Tokui T, Abe T, Ikeda T and Nishimura K (2001) Human liver-specific organic anion transporter, LST-1, mediates uptake of pravastatin by human hepatocytes. *J Pharmacol Exp Ther* 297: 861-867.

Niemi M, Pasanen MK and Neuvonen PJ (2011) Organic anion transporting polypeptide 1B1: a genetically polymorphic transporter of major importance for hepatic drug uptake. *Pharmacol Rev* 63: 157-181.

Nies AT and Keppler D (2007) The apical conjugate efflux pump ABCC2 (MRP2). *Pflugers Arch: Euro J Physio* 453: 643-659.

Pressler H, Sissung TM, Venzon D, Price DK and Figg WD (2011) Expression of OATP family members in hormone-related cancers: potential markers of progression. *PLoS One* 6: e20372.

Rodgers T, Leahy D, and Rowland M (2005) Physiologically based pharmacokinetic modeling 1: predicting the tissue distribution of moderate-to-strong bases. *J Pharm Sci* 94:1259-1276.

Rodgers T and Rowland M (2006) Physiologically based pharmacokinetic modelling 2: predicting the tissue distribution of acids, very weak bases, neutrals and zwitterions. *J Pharm Sci* 95:1238-1257.

Rodgers T and Rowland M (2007) Mechanistic approaches to volume of distribution predictions: understanding the processes. *Pharm Res* 24:918-933.

Swift B, Pfeifer ND and Brouwer KL (2010) Sandwich-cultured hepatocytes: an in vitro model to evaluate hepatobiliary transporter-based drug interactions and hepatotoxicity. *Drug Metab Rev* 42: 446-471.

Takashima T, Kitamura S, Wada Y, Tanaka M, Shigihara Y, Ishii H, Ijuin R, Shiomi S, Nakae T, Watanabe Y, Cui Y, Doi H, Suzuki M, Maeda K, Kusuhara H, Sugiyama Y and Watanabe Y (2012) PET

672 imaging-based evaluation of hepatobiliary transport in humans with (15R)-11C-TIC-Me. *J Nucl Med* 53:
673 741-748.
674 Tang YQ and Weng N (2013) Salting-out assisted liquid-liquid exraction for bioanalysis. *Bioanalysis* 5:
675 1583-1598.
676 Varma MV, Lai Y, Kimoto E, Goosen TC, El-Kattan AF and Kumar V (2013) Mechanistic modeling to
677 predict the transporter- and enzyme-mediated drug-drug interactions of repaglinide. *Pharm Res* 30: 1188-
678 1199.
679 Varma MV, Steyn SJ, Allerton C and El-Kattan AF (2015) Predicting Clearance Mechanism in Drug
680 Discovery: Extended Clearance Classification System (ECCS). *Pharm Res* 32: 3785-3802.
681 Wang Q, Zheng M and Leil T (2017) Investigating Transporter-Mediated Drug-Drug Interactions Using a
682 Physiologically Based Pharmacokinetic Model of Rosuvastatin. *CPT Pharmacometrics Syst Pharmacol* 6:
683 228-238.
684 Watanabe T, Kusuhara H, Maeda K, Shitara Y and Sugiyama Y (2009) Physiologically based
685 pharmacokinetic modeling to predict transporter-mediated clearance and distribution of pravastatin in
686 humans. *J Pharmacol Exp Ther* 328: 652-662.
687 Wlcek K, Svoboda M, Thalhammer T, Sellner F, Krupitza G and Jaeger W (2008) Altered expression of
688 organic anion transporter polypeptide (OATP) genes in human breast carcinoma. *Cancer Biol Ther* 7:
689 1450-1455.
690 Woo SR, Fuertes MB, Corrales L, Spranger S, Furdyna MJ, Leung MY, Duggan R, Wang Y, Barber GN,
691 Fitzgerald KA, Alegre ML, Gajewski TF (2014) STING-dependent cytosolic DNA sensing mediates
692 innate immune recognition of immunogenic tumors. *Immunity* 41: 830-842.
693 Yang F, Liu L, Chen L, Liu M, Liu F, Xiong Y, Hu X and Xia C (2018) OATP1B3 (699G>A) and
694 CYP2C9*2, *3 significantly influenced the transport and metabolism of glibenclamide and glipizide.
695 *Scientific Reports* 8:18063.
696 Yoshikado T, Toshimoto K, Maeda K, Kusuhara H, Kimoto E, Rodrigues AD, Chiba K and Sugiyama Y
697 (2018) PBPK Modeling of Coproporphyrin I as an Endogenous Biomarker for Drug Interactions

698 Involving Inhibition of Hepatic OATP1B1 and OATP1B3. *CPT: Pharmacometrics Syst Pharmacol* 7:
699 739-747.

700

Figure Legends

Figure 1: Structure of E7766, a novel agonist of STING pathway

Figure 2: Phenotyping of hepatobiliary transporters involved in the disposition of E7766. (2A) Uptake of E7766 was evaluated in SLC transporter-expressing HEK293 cells; (2B) Transport of E7766 was evaluated on ABC transporter-expressing membrane vesicles.

Figure 3: In vitro transporter kinetics of E7766 were measured in HEK-293 cells expression OATP1B1 or OATP1B3. (3A) Kinetics and Michaelis-menten parameters of OATP1B1-mediated uptake of E7766; (3B) Kinetics and Michaelis-menten parameters of OATP1B3-mediated uptake of E7766.

Figure 4: Pharmacokinetics and disposition of E7766 following intravenous administration in wild type and OATP1B1/1B3 humanized mice. (4A) Plasma concentrations of E7766 were measured with or without coadministration with Rifampicin following intravenous administration of E7766 and Rifampicin. (4B) Blood concentrations of E7766 were measured with or without coadministration with Rifampicin following intravenous administration of E7766 and Rifampicin. (4C) Excretion with or without coadministration with Rifampicin of E7766 in urine, bile and feces was determined following intravenous administration of E7766 and Rifampicin. (WT: wild type mouse; Hu: Humanized mouse)

Figure 5 Summary of PK parameters and DDI profile of E7766 from PBPK model. (5A) Contribution of passive diffusion, OATP1B1 and OATP1B3-mediated uptake to overall hepatic uptake clearance of E7766. Simulated plasma (5B) and liver (5C) concentration-time profiles of E7766 following i.v. administration of 1 mg dose with and without 600 mg oral dose of

723 Rifampicin. Sensitivity analysis of changes in E7766 area under the curve ratio (AUCR) as a
724 function of REF (5D) and kinetic parameters for OATP1B1 (5E) and OATP1B3 (5F).

725

DMD Fast Forward. Published on December 18, 2020 as DOI: 10.1124/dmd.120.000125
This article has not been copyedited and formatted. The final version may differ from this version.

Tables

Table 1

Summary of in vitro parameters for E7766 estimated from the sandwich cultured human hepatocytes

Test Article	Target Concentration (μmol/L)	Temperature	Time (min)	Uptake $CL_{int,T}$ (μL/min/10^6 cells)	Efflux $CL_{int,T}$ (μL/min/10^6 cells)	BEI %
E7766	0.3	37°C	1	7.69 ± 0.47	—	—
			5	3.83 ± 0.26	—	—
			10	3.12 ± 0.26	—	—
			20	Not determined	2.05 ± 0.07	85.2 ± 1.7
		4°C	10	0.13 ± 0.00	—	—
	1.0	37°C	1	5.46 ± 0.10	—	—
			5	2.70 ± 0.14	—	—
			10	1.85 ± 0.13	—	—
			20	Not determined	1.42 ± 0.08	86.2 ± 0.40
		4°C	10	0.14 ± 0.02	—	—
	10.0	37°C	1	1.22 ± 0.11	—	—
			5	0.47 ± 0.02	—	—
			10	0.33 ± 0.01	—	—
			20	Not determined	0.15 ± 0.01	70.9 ± 1.3
		4°C	10	0.58 ± 0.73	—	—
d8-TCA	5	37°C	10	14.2 ± 0.82	11.0 ± 1.74	72.6 ± 5.8
		4°C		0.27 ± 0.02	—	—
Rosuvastatin	10	37°C	10	6.22 ± 0.31	2.23 ± 0.38	42.7 ± 5.8
		4°C		0.21 ± 0.04	—	—

Uptake $CL_{int,T}$, intrinsic hepatic uptake clearance; Efflux $CL_{int,T}$, intrinsic biliary efflux clearance; BEI, biliary excretion index; d8-TCA, deuterium-labeled sodium taurocholate. Values represent the means ± SD (n = 3)

DMD Fast Forward. Published on December 18, 2020 as DOI: 10.1124/dmd.120.000125
This article has not been copyedited and formatted. The final version may differ from this version.

Table 2

Disposition of E7766 in bile duct cannulated (BDC) rat and dog following intravenous bolus administration

Dose	**BDC Rat IV bolus, 1 mg/kg**	**Dog IV bolus, 0.075 mg/kg**
$CL_{tot,p}$ (L/h/kg)	6.50 ± 0.429	1.29 ± 0.369
V_{ss} (L/kg)	2.47 ± 0.849	0.553 ± 0.345
$A_{e\ renal}$ (%)	13.7 ± 2.80	4.96 ± 4.37
CL_{renal} (L/h/kg)	0.895 ± 0.189	0.0528 ± 0.0293
$A_{e\ biliary}$ (%)	92.1 ± 7.26	87.9 ± 30.5
$CL_{biliary}$ (L/h/kg)	6.04 ± 0.798	1.19 ± 0.637
$A_{e\ fecal}$ (%)	0.366 ± 0.208	—
CL_{fecal} (L/h/kg)	0.0227 ± 0.0138	—

$CL_{tot,p}$, total plasma clearance; V_{ss}, distribution volume at steady state; $A_{e\ renal}$, amount excreted in urine; CL_{renal}, renal excretory clearance; $A_{e\ biliary}$, amount excreted in bile; $CL_{biliary}$, hepatobiliary excretory clearance; $A_{e\ fecal}$, amount excreted in feces; CL_{fecal}, fecal excretory clearance. Values represent the means ± SD (n = 4 for BDC rats and n = 3 for dogs)

DMD Fast Forward. Published on December 18, 2020 as DOI: 10.1124/dmd.120.000125
This article has not been copyedited and formatted. The final version may differ from this version.

Table 3

Liver and systemic exposure of E7766 in wild type and humanized mice in the presence or the absence of Rifampicin.

Parameters	**WT Mice 0.5 mg/kg E7766**	**WT Mice 0.5 mg/kg E7766 +Rifampicin**	**Hu Mice 1.0 mg/kg E7766**	**Hu Mice 0.5 mg/kg E7766 +Rifampicin**
AUC_{total} (ng·h/mL)	56.0	300	126 ± 48.7	302 ± 92.2
AUC_{total}/Dose (ng·h/mL/[mg/kg])	112	600	126 ± 48.7	604 ± 184
$CL_{tot,p}$ (L/h/kg)	8.93	1.72	9.20 ± 4.65	1.80 ± 0.619
V_{ss} (L/kg)	1.66	0.520	5.93 ± 5.96	1.29 ± 0.243
Liver AUC_{total} (ng·h/g)	4460	4250	—	—
Liver $K_{p,total}$	79.6	14.2	—	—

WT, Wild type mouse; Hu, OATP1B1/OATP1B3 humanized mouse; AUC_{total}, area under the total plasma concentration-time curve; AUC_{total}/Dose, area under the total plasma concentration-time curve normalized by dose; $CL_{tot,p}$, total plasma clearance; V_{ss}, distribution volume at steady state; Liver AUC_{total}, area under the total liver concentration-time curve; Liver $K_{p,total}$, total liver-to-plasma concentration ratio. Values represent the means ± SD (n = 3)

Table 4

Summary of input parameters used to build the PBPK model for E7766.

Parameter	Scenario one	Scenario two	Source
PhysChem and Blood Binding			
Mol Weight (g/mol)	746	746	Calculated
log P	1.31	1.31	Measured
Compound Type	Monoprotic Acid	Monoprotic Acid	—
pKa	3.41	3.41	Calculated
B/P	0.55	0.55	Measured
f_u	0.50	0.50	Measured
Distribution Model	Full PBPK Model	Full PBPK Model	—
V_{ss} (L/kg)	0.637	0.637	SimCYP predicted (Method 2, the Rodgers-Rowland method)
K_p scalar	4.0	4.0	fitted based on preclinical data, see Methods for details
CL_{renal} (L/h)	3.0	3.0	Estimate as f_u × GFR
Hepatic Transport (permeability-limited liver module)			
Passive diffusion CL_{PD} (mL/min/10^6 cells)	0.00013	0.00013	Obtained from E7766 uptake measured at 0.3 μmol/L at 4 °C with SCHH model (Table 1)
fuIW	1.00	1.00	SimCYP predicted
fuEW	0.657	0.657	SimCYP predicted

J_{max} (pmol/min/10^6 cells) for OATP1B1	8.34	—	V_{max} in the unit of pmol/min/mg protein (Figure 3) was converted to J_{max} in the unit pmol/min/10^6 cells by incorporating measured protein abundance data of HEK293 cells (0.3 mg protein per 10^6 HEK293 cells)
K_m (µmol/L) for OATP1B1	2.20	—	Obtained from transporter kinetic assays (Figure 3)
f_{uinc} for OATP1B1	1.00	—	SimCYP predicted
REF for OATP1B1	0.10	—	Calculated by Equation 4, see Supplemental Table 2 for details of transporter protein expression.
J_{max} (pmol/min/10^6 cells) for OATP1B3	24.39	—	Figure 3. Units were converted as shown above for OATP1B1
K_m (µmol/L) for OATP1B3	3.97	—	Obtained from transporter kinetic assays (Figure 3)
f_{uinc} for OATP1B3	1.00	1.00	SimCYP predicted
REF for OATP1B3	2.80	—	Calculated by Equation 5, see Supplemental Table 2 for details of transporter protein expression.
Uptake $CL_{int,T}$ (µL/min/10^6 cells)	—	7.7	For scenario two, the uptake $CL_{int,T}$ for E7766 measured at 0.3 µmol/L after 1 min incubation at 37 °C (Table 1) was assigned as input value for uptake $CL_{int,T}$ in SCHH, as early time point and lower concentration can better represent the initial linear uptake phase.
REF_{SCHH}	—	1	The REF_{SCHH} is assumed to be one based on literature reported data shown that OATP1B1 and OATP1B3 expression levels are comparable between SCHH and primary hepatocyte if from the same lot (Kimoto et al., 2012)
Efflux $CL_{int,T}$ (µL/min/10^6 cells)	2.1	2.1	For both scenarios one and two, SCHH efflux $CL_{int,T}$ for E7766 measured at 0.3 µmol/L after 20 min incubation at 37 °C (Table 1) was used as input value for Efflux $CL_{int,T}$.

B/P, blood-to-plasma partition ratio; f_u, unbound drug fraction in plasma; V_{ss}, distribution volume at steady state; K_p, tissue-to-plasma partition coefficients ; CL_{renal}, renal excretory clearance; CL_{PD}, passive diffusion clearance ; fuIW, unbound drug fraction in intracellular water; fuEW, unbound drug fraction in extracellular water; f_{uinc}, unbound drug fraction in in-vitro incubation system; K_m, Michaelis-Menten constant; J_{max}, in vitro maximum rate of transporter mediate uptake or efflux; REF, relative

expression factor; Uptake $CL_{int,T}$, intrinsic uptake clearance obtained from SCHH assay; Efflux $CL_{int,T}$, intrinsic biliary efflux clearance obtained from SCHH assay. For scenario one, hepatic uptake clearance was assigned from the transporter kinetics measured in HEK 293 cells and for scenario two, intrinsic active uptake clearance measured in from SCHH was assigned to OATP1B3.

DMD Fast Forward. Published on December 18, 2020 as DOI: 10.1124/dmd.120.000125
This article has not been copyedited and formatted. The final version may differ from this version.

Table 5

Summary and comparison of simulated PK and DDI parameters of E7766 from PBPK models using two scenarios. Simcyp default compound for rifampicin was used for simulations. For scenario one, hepatic uptake clearance was assigned from the transporter kinetics measured in HEK 293 cells and for scenario two, intrinsic active uptake clearance measured in from SCHH was assigned to OATP1B3.

PKPD profile parameters of E7766	**Scenario one**		**Scenario two**	
	(-) Rifampicin	**(+) Rifampicin**	**(-) Rifampicin**	**(+) Rifampicin**
AUC_{total} (nmol·h/L)	47.38	131.06	67.26	174.07
AUC_{total} ratio	2.77		2.59	
$C_{max,tot}$ (nmol/L)	474.01	479.92	476.24	480.12
$C_{max,tot}$ ratio	1.01		1.01	
$CL_{tot,p}$ (L/h)	29.62	11.88	21.55	8.66
$CL_{tot,p}$ ratio	0.40		0.40	
Liver intracellular AUC_{free} (nmol·h/L)	76.19	69.06	71.35	61.28
Liver intracellular AUC_{free} ratio	0.91		0.86	

AUC_{total}, area under total plasma concentration-time curve; AUC_{total} ratio, ratio of AUC_{total} in the presence and absence of the inhibitor; $C_{max,tot}$ maximum total plasma concentration; $C_{max,tot}$ ratio, ratio of $C_{max,tot}$ in the presence and absence of the inhibitor; $CL_{tot,p}$, total plasma clearance; $CL_{tot,p}$ ratio, ratio of $CL_{tot,}$ in the presence and absence of the inhibitor; Liver intracellular AUC_{free}, area under free intra-hepatocellular concentration-time curve; Liver intracellular AUC_{free} ratio, ratio of area under free intra-hepatocellular concentration-time curve in the presence and absence of the inhibitor.

DMD Fast Forward. Published on December 18, 2020 as DOI: 10.1124/dmd.120.000125
This article has not been copyedited and formatted. The final version may differ from this version.

Figures

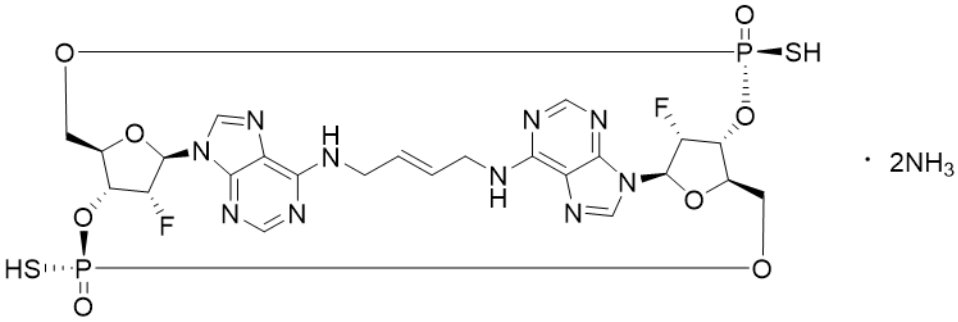

Figure 1

DMD Fast Forward. Published on December 18, 2020 as DOI: 10.1124/dmd.120.000125
This article has not been copyedited and formatted. The final version may differ from this version.

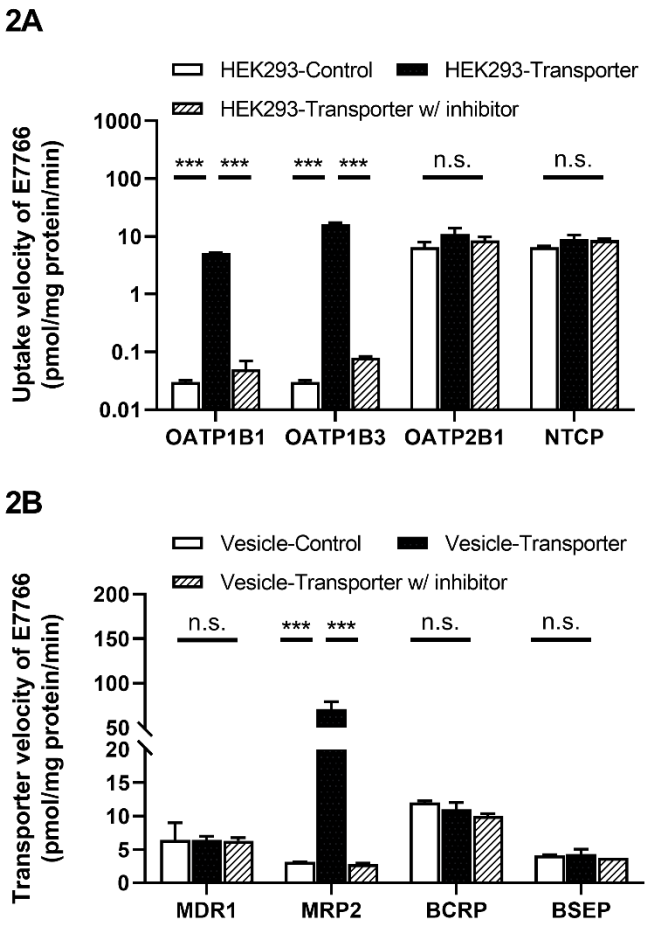

Figure 2

DMD Fast Forward. Published on December 18, 2020 as DOI: 10.1124/dmd.120.000125
This article has not been copyedited and formatted. The final version may differ from this version.

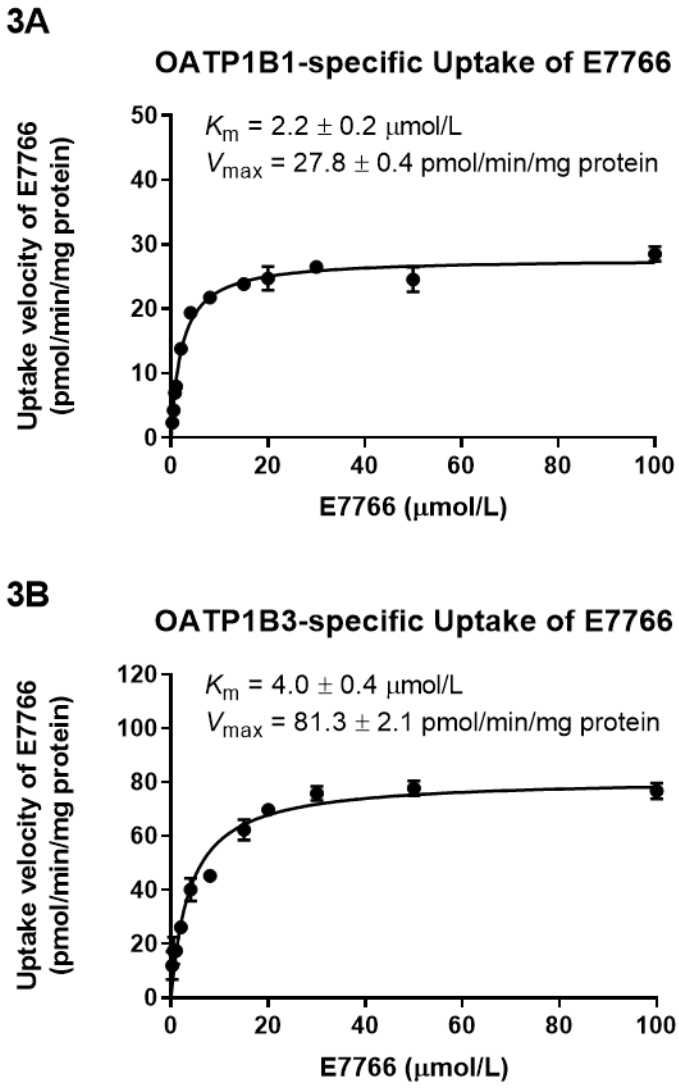

Figure 3

DMD Fast Forward. Published on December 18, 2020 as DOI: 10.1124/dmd.120.000125
This article has not been copyedited and formatted. The final version may differ from this version.

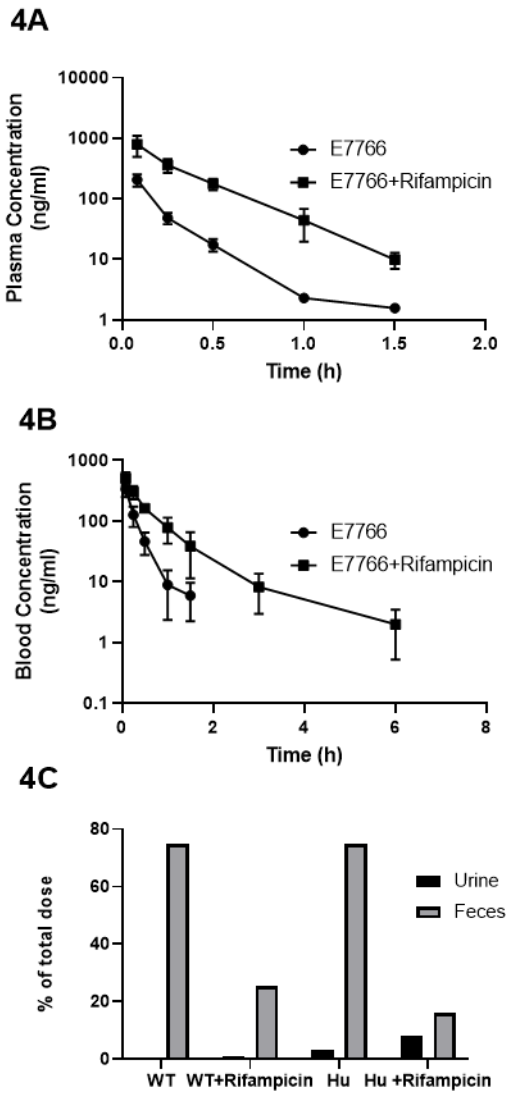

Figure 4

DMD Fast Forward. Published on December 18, 2020 as DOI: 10.1124/dmd.120.000125
This article has not been copyedited and formatted. The final version may differ from this version.

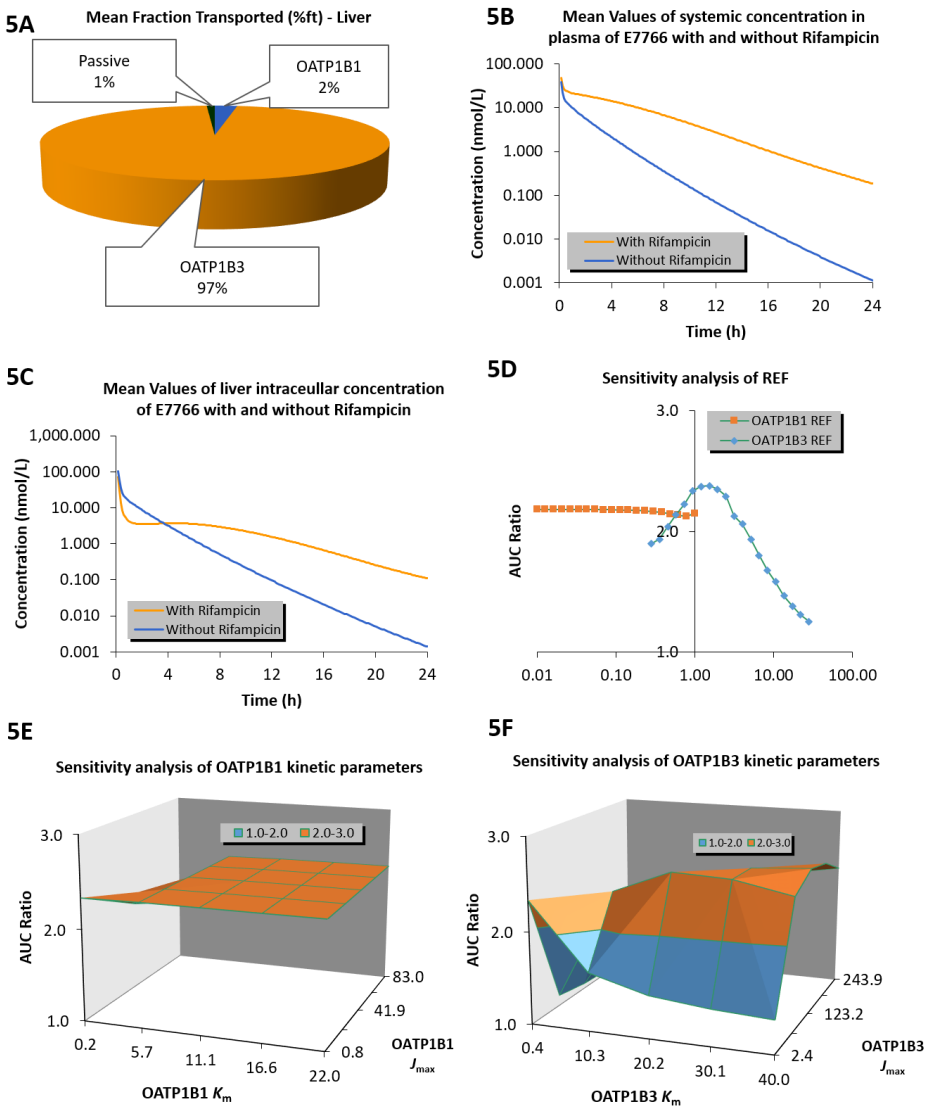

Figure 5

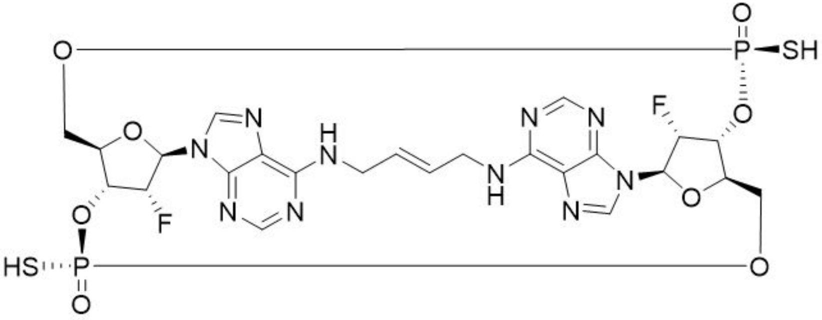

· $2NH_3$

2A

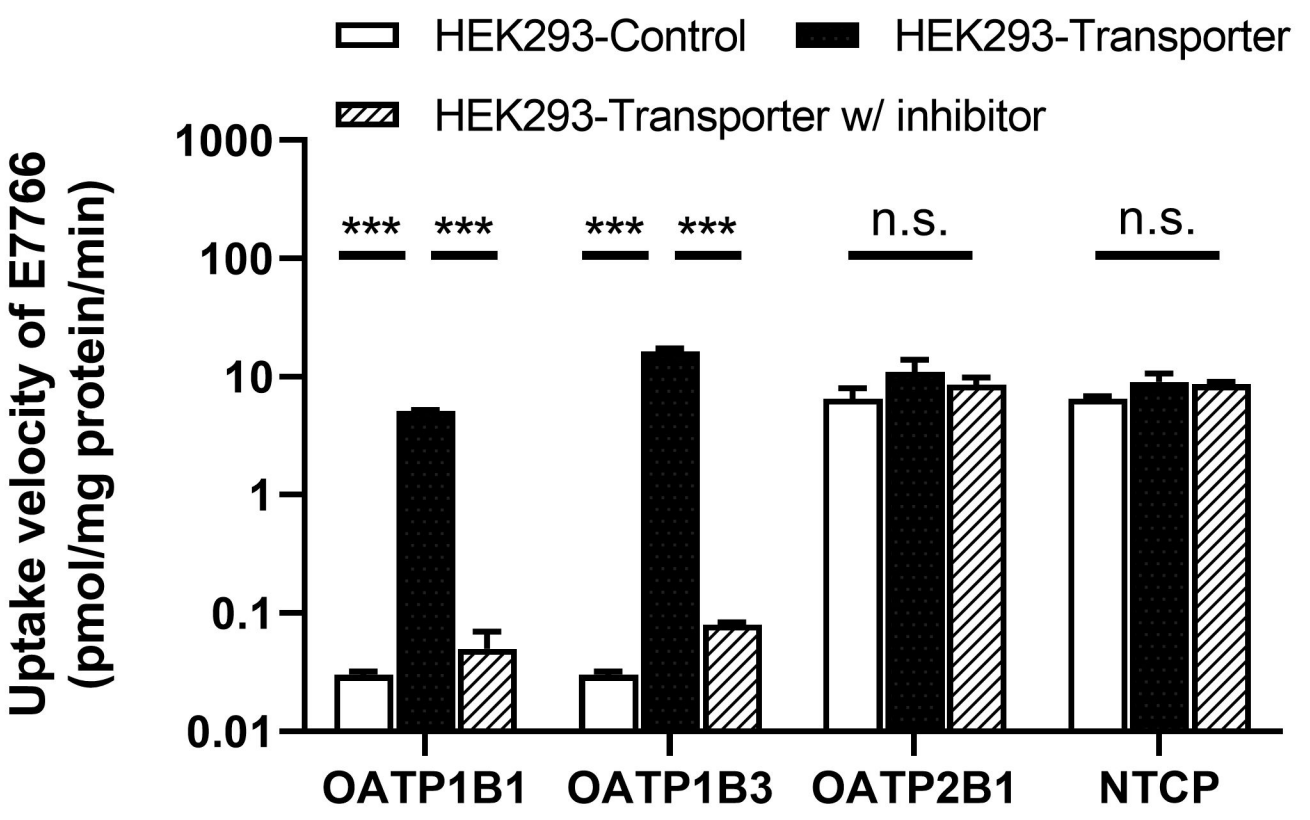
HEK293-Control
HEK293-Transporter
HEK293-Transporter w/ inhibitor
Uptake velocity of E7766 (pmol/mg protein/min)
1000
100
10
1
0.1
0.01
*** *** *** *** n.s. n.s.
OATP1B1
OATP1B3
OATP2B1
NTCP

2B

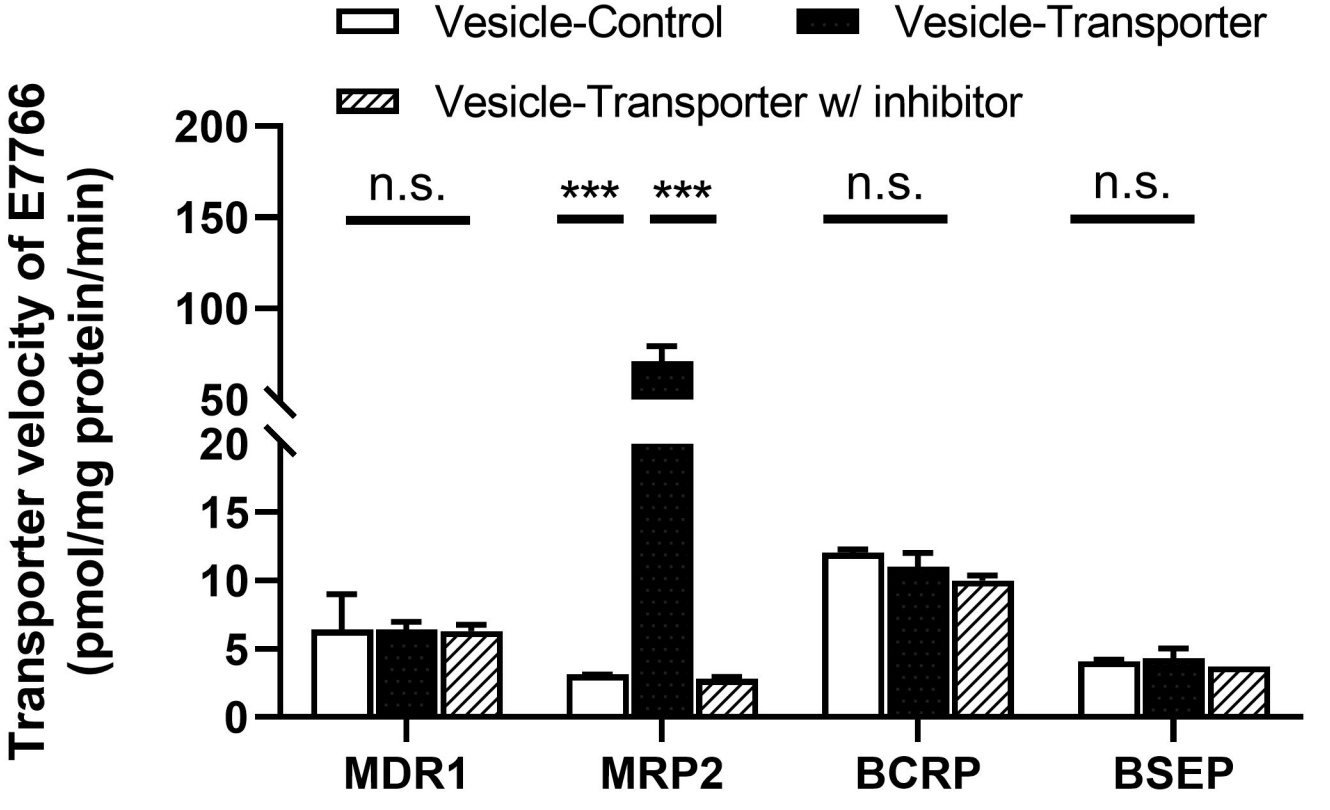
Vesicle-Control
Vesicle-Transporter
Vesicle-Transporter w/ inhibitor
Transporter velocity of E7766 (pmol/mg protein/min)
200
150
100
50
20
15
10
5
0
n.s. *** *** n.s. n.s.
MDR1
MRP2
BCRP
BSEP

3A

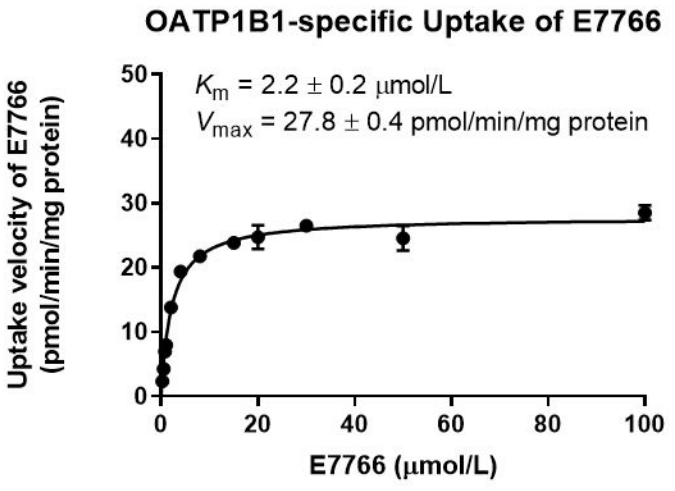
OATP1B1-specific Uptake of E7766
K_m = 2.2 ± 0.2 μmol/L
V_{max} = 27.8 ± 0.4 pmol/min/mg protein
Uptake velocity of E7766 (pmol/min/mg protein)
E7766 (μmol/L)
0
10
20
30
40
50
0
20
40
60
80
100

3B

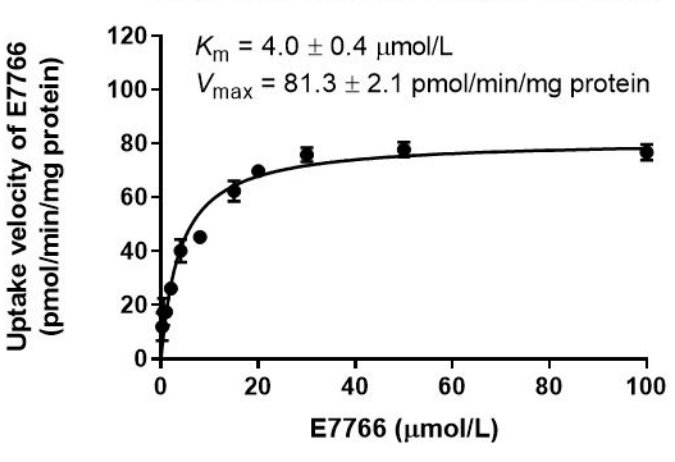
OATP1B3-specific Uptake of E7766
K_m = 4.0 ± 0.4 μmol/L
V_{max} = 81.3 ± 2.1 pmol/min/mg protein
Uptake velocity of E7766 (pmol/min/mg protein)
E7766 (μmol/L)
0
20
40
60
80
100
120
0
20
40
60
80
100

4A

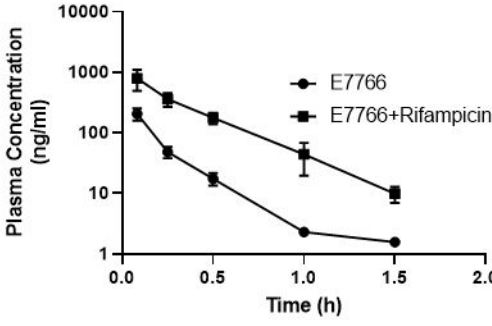
Plasma Concentration (ng/ml)
10000
1000
100
10
1
E7766
E7766+Rifampicin
0.0
0.5
1.0
1.5
2.0
Time (h)

4B

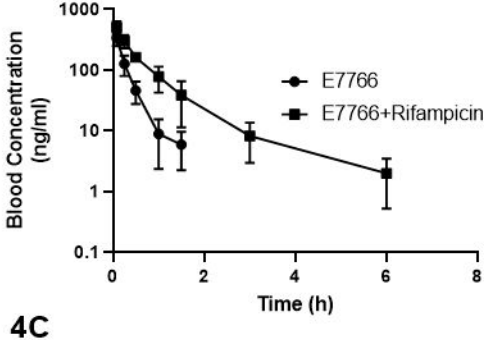
Blood Concentration (ng/ml)
1000
100
10
1
0.1
E7766
E7766+Rifampicin
0
2
4
6
8
Time (h)

4C

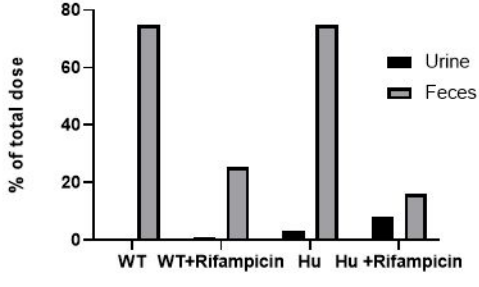
% of total dose
80
60
40
20
0
Urine
Feces
WT
WT+Rifampicin
Hu
Hu +Rifampicin

DMD Fast Forward. Published on December 18, 2020 as DOI: 10.1124/dmd.120.000125
This article has not been copyedited and formatted. The final version may differ from this version.

5A

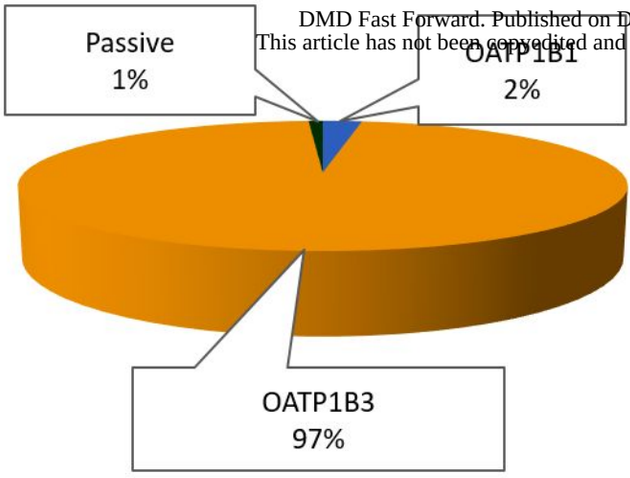

5B

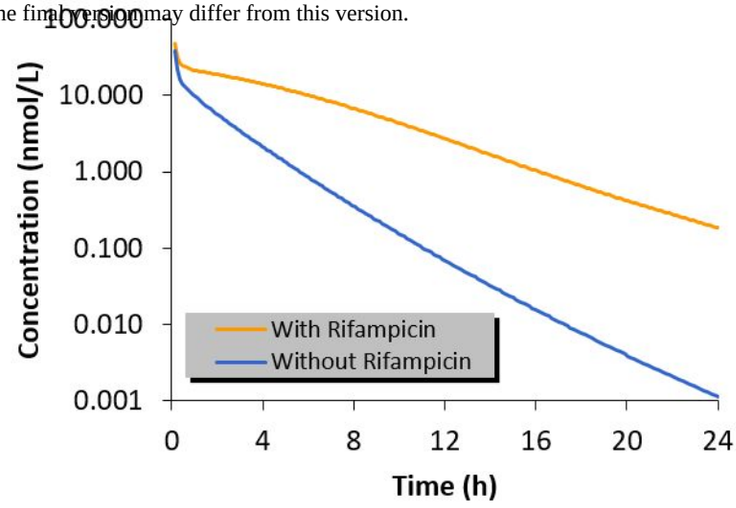

5C

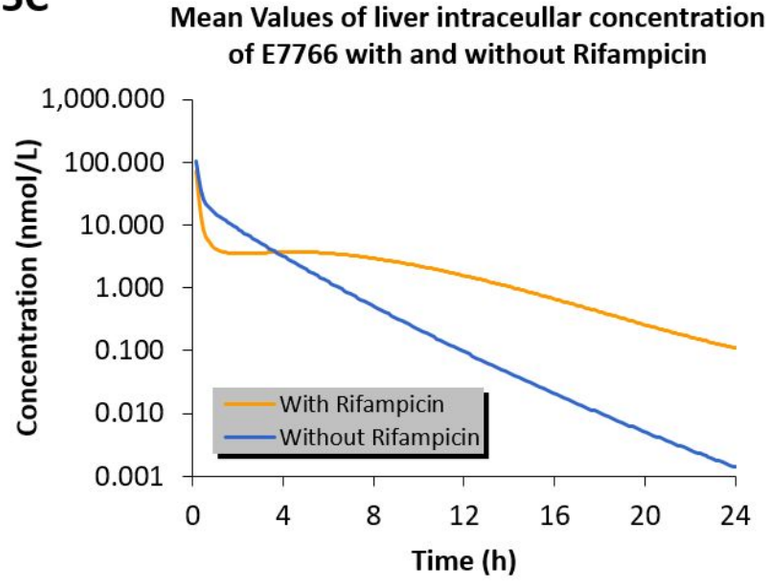

5D

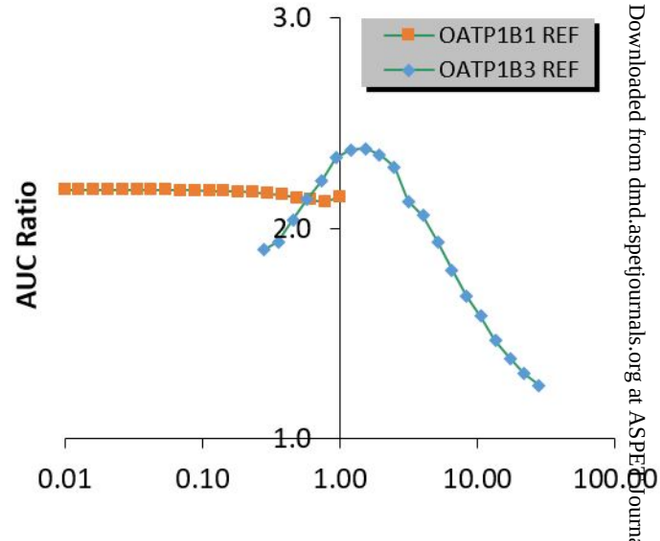

5E

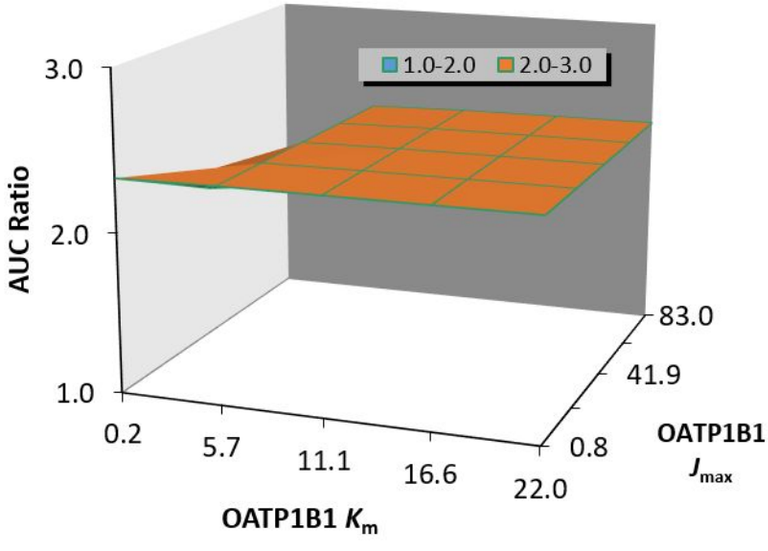

5F

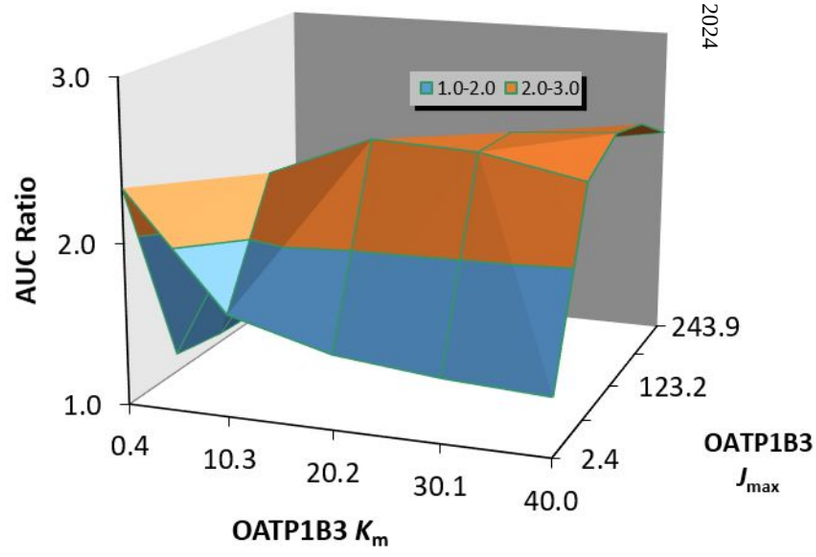

Manuscript number: DMD-AR-2020-000125R2

Prediction of transporter-mediated drug-drug interactions and phenotyping of hepatobiliary transporters involved in the clearance of E7766, a novel macrocycle-bridged dinucleotide

Rongrong Jiang[*], Andrew Hart[1], Laurette Burgess, Dae-Shik Kim, Weidong Lai[2], Vaishali Dixit[*]

Drug Metabolism and Pharmacokinetics, Eisai Inc, Massachusetts, USA (R.J., V.D., G.L., A.H.)

Genetics Guided Dementia Discovery, Eisai Inc, Massachusetts, USA (L.B., DS.K.)

[1]Current Address: Wave Life Sciences, Massachusetts, USA

[2]Current Address: Triplet Therapeutics, Massachusetts, USA

[*]Co-corresponding authors

Running Title: Transporter-mediated drug-drug interactions for E7766

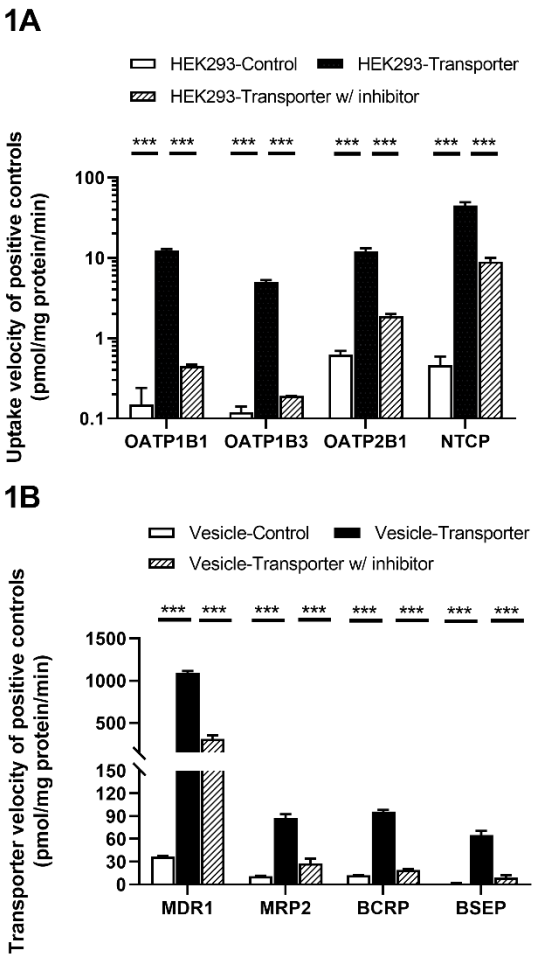

Supplemental Figure 1 Uptake activity of positive controls in the presence and absence of inhibitors in uptake transporter-expressing cells (A) or efflux transporter-expressing vesicles (B). Estradiol 17-β-glucuronide ($E_2$17βG, 10 μmol/L) was used as positive control and Rifampicin (100 μmol/L) was used as inhibitor for OATP1B1 and OATP1B3; [^{3}H]Taurocholic acid (TCA, 2 μmol/L) and Troglitazone (100 μmol/L) were used as positive control and inhibitor for NTCP; [^{3}H]Estrone-3-Sulfate (E3S, 2 μmol/L) and Rifamycin SV (100 μmol/L) were used as positive control and inhibitor for OATP2B1; N-methyl-quinidine (2 μmol/L) and Ketoconazole (20 μmol/L) were used as positive control and inhibitor for MDR1; [^{3}H]$E_2$17βG (10 μmol/L) and MK571 (100 μmol/L) were used as positive control and inhibitor for MRP2, respectively;

39 [^{3}H]E3S (2 μmol/L) and Novobiocin (3 μmol/L) were used as positive control and inhibitor for
40 BCRP; [^{3}H]TCA (1 μmol/L) and Ketoconazole (20 μmol/L) were used as positive control and
41 inhibitor for BSEP. All experiments were run in triplicates.

Manuscript number: DMD-AR-2020-000125R2

Prediction of transporter-mediated drug-drug interactions and phenotyping of hepatobiliary transporters involved in the clearance of E7766, a novel macrocycle-bridged dinucleotide

Rongrong Jiang[*], Andrew Hart[1], Laurette Burgess, Dae-Shik Kim, Weidong Lai[2], Vaishali Dixit[*]

Drug Metabolism and Pharmacokinetics, Eisai Inc, Massachusetts, USA (R.J., V.D., G.L., A.H.)

Genetics Guided Dementia Discovery, Eisai Inc, Massachusetts, USA (L.B., DS.K.)

[1]Current Address: Wave Life Sciences, Massachusetts, USA

[2]Current Address: Triplet Therapeutics, Massachusetts, USA

[*]Co-corresponding authors

Running Title: Transporter-mediated drug-drug interactions for E7766

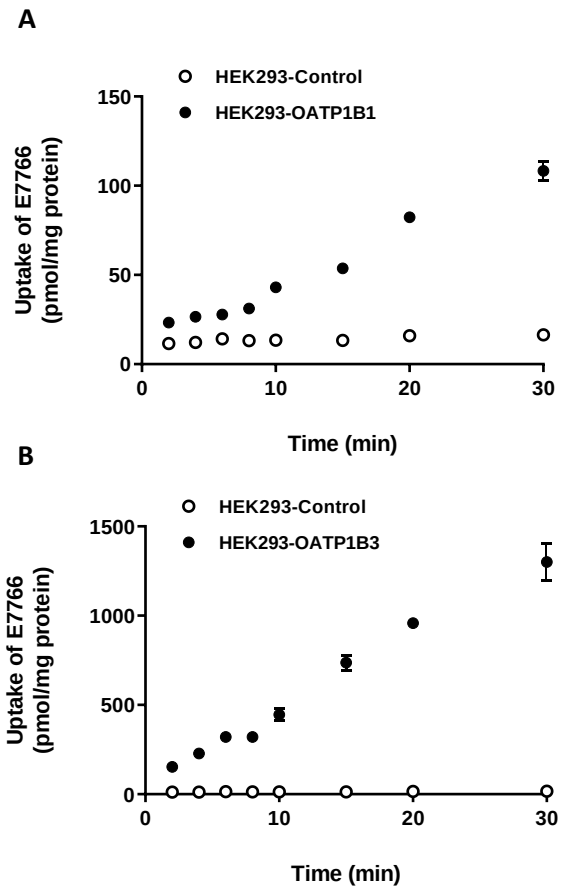

Supplemental Figure 2 Time-dependent uptake of E7766 with HEK293-control (empty circle, A, B), HEK293-OATP1B1 (solid circle, A) and HEK293-OAPT1B3 (solid circle, B) cells. All experiments were run in triplicates.

Manuscript number: DMD-AR-2020-000125R2

Prediction of transporter-mediated drug-drug interactions and phenotyping of hepatobiliary transporters involved in the clearance of E7766, a novel macrocycle-bridged dinucleotide

Rongrong Jiang[*], Andrew Hart[1], Laurette Burgess, Dae-Shik Kim, Weidong Lai[2], Vaishali Dixit[*]

Drug Metabolism and Pharmacokinetics, Eisai Inc, Massachusetts, USA (R.J., V.D., G.L., A.H.)

Genetics Guided Dementia Discovery, Eisai Inc, Massachusetts, USA (L.B., DS.K.)

[1]Current Address: Wave Life Sciences, Massachusetts, USA

[2]Current Address: Triplet Therapeutics, Massachusetts, USA

[*]Co-corresponding authors

Running Title: Transporter-mediated drug-drug interactions for E7766

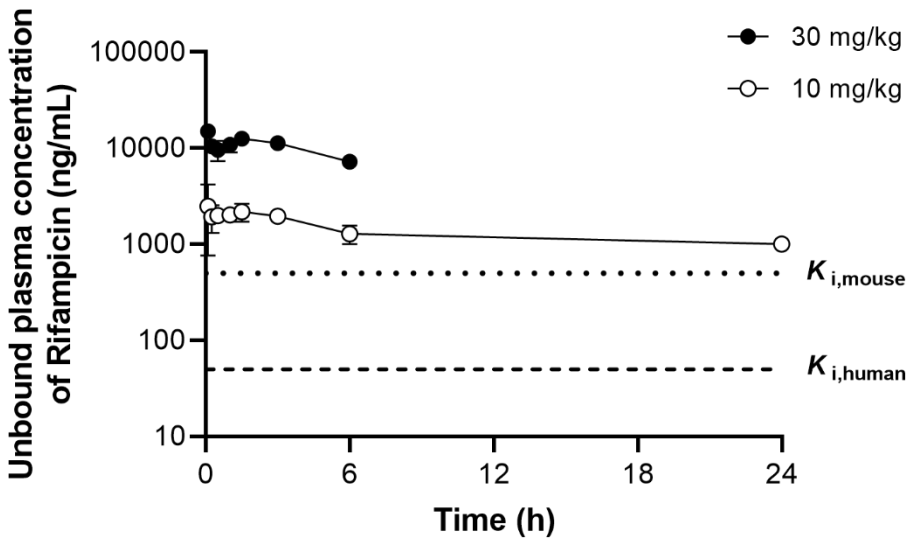

Supplemental Figure 3 Systemic unbound concentration versus time profile of Rifampicin in mice after i.v. bolus coadministration of E7766 and Rifampicin. Data are presented as mean ± SD (N=3). $K_{i,human}$ was adapted from K_i value incorporated in SimCYP for human 1B1/1B3 inhibition while $K_{i,mouse}$ was assumed as half of the reported IC_{50} value against murine Oatp1b2 (Bins, et al., 2017).

Reference

Bins S, van Doom L, Phelps MA, Gibson AA, Hu S, Li L, *et al.* (2017). Influence of OATP1B1 Function on the Disposition of Sorafenib-β-D-Glucuronide. Clin Transl Sci 10**:** 271-279.

Manuscript number: DMD-AR-2020-000125R2

Prediction of transporter-mediated drug-drug interactions and phenotyping of hepatobiliary transporters involved in the clearance of E7766, a novel macrocycle-bridged dinucleotide

Rongrong Jiang[*], Andrew Hart[1], Laurette Burgess, Dae-Shik Kim, Weidong Lai[2], Vaishali Dixit[*]

Drug Metabolism and Pharmacokinetics, Eisai Inc, Massachusetts, USA (R.J., V.D., G.L., A.H.)

Genetics Guided Dementia Discovery, Eisai Inc, Massachusetts, USA (L.B., DS.K.)

[1]Current Address: Wave Life Sciences, Massachusetts, USA

[2]Current Address: Triplet Therapeutics, Massachusetts, USA

[*]Co-corresponding authors

Running Title: Transporter-mediated drug-drug interactions for E7766

Supplemental Table 1 Permeability assessment of E7766 in LLC-PK1 cells.

	Testing concentration (μmol/L)	P_{app}[a], **A-B (×10^{-6} cm/s)**	P_{app}, **B-A (×10^{-6} cm/s)**
E7766	3	BLOQ[b]	0.61 ± 0.14
E7766	10	0.40 ± 0.04	0.29 ± 0.07

[a]P_{app}, apparent cell-based membrane permeability; P_{app} was calculated by following equation,

P_{app} ($\times 10^{-6}$ cm/s) = $C_{rec,end}/C_{donor,ini} \times$ Receiver V/Δt/A$\times 10^6$,

Where $C_{rec,end}$ is the concentration of compound in the receiver compartment at the end of incubation (nmol/L); $C_{donor,ini}$ is the initial concentration in donor compartment (nmol/L); Receiver V is the solution volume (mL) in the receiver compartment; Δt is the incubation time (min); A is the surface area of insert membrane (0.14 cm^2).

[b]BLOQ, below the limit of quantification (0.2 nmol/L)

The compound showed minimal non-specific binding to the assay plate as demonstrated by the high recovery (93-110%); Values represent the means ± SD (n = 6)

Manuscript number: DMD-AR-2020-000125R2

Prediction of transporter-mediated drug-drug interactions and phenotyping of hepatobiliary transporters involved in the clearance of E7766, a novel macrocycle-bridged dinucleotide

Rongrong Jiang[*], Andrew Hart[1], Laurette Burgess, Dae-Shik Kim, Weidong Lai[2], Vaishali Dixit[*]

Drug Metabolism and Pharmacokinetics, Eisai Inc, Massachusetts, USA (R.J., V.D., G.L., A.H.)

Genetics Guided Dementia Discovery, Eisai Inc, Massachusetts, USA (L.B., DS.K.)

[1]Current Address: Wave Life Sciences, Massachusetts, USA

[2]Current Address: Triplet Therapeutics, Massachusetts, USA

[*]Co-corresponding authors

Running Title: Transporter-mediated drug-drug interactions for E7766

Supplemental Table 4 Summary of input parameters of Rifampicin used to conduct drug-drug interaction simulation of E7766

Compound Name	**Rifampicin**
Route	Oral
Dose	600 mg
PhysChem and Blood Binding	
Mol Weight (g/mol)	823.000
log P	4.010
Compound Type	Ampholyte
pKa 1	1.700
pKa 2	7.900
B/P	0.900
f_u	0.116
Absorption Model	ADAM
Input type	Predicted
f_a	0.925
k_a (1/h)	0.939
f_u(Gut)	1.000
$P_{eff,man}$ Type	Global
$P_{eff,man}$ (10^{-4} cm/s)	2.151
$P_{eff,man}$ Cap (10^{-4} cm/s)	12.000
Permeability Assay	Caco-2
Apical pH : Basolateral pH	6.5 : 7.4
Activity	Passive
PCaco-2(10E-06 cm/s)	15.000
Distribution Model	Full PBPK Model
V_{ss} (L/kg)	0.420
Prediction Method	Method 2
K_p Scalar	0.098
Elimination	
Additional HLM CL_{int} (μL/min/mg protein)	2.840
Biliary CL_{int} (Hep) (μL/min/10^6)	0.288
Percentage available for re-absorption (%)	100.000
Active Hepatic Scalar (Net)	1.000
CL_{renal} (L/h)	1.260
CYPs and/or UGTs Interaction	
Enzyme	CYP2C8
K_i (μM)	24.500
Enzyme	CYP3A4

K_i (µM)	15.000
$f_{u,mic}$	1.000
Transporters Interaction	
Organ/Tissue	Gut
Transporter	ABCB1 (P-gp/MDR1)
K_i (µM)	23.800
Transporter	ABCG2 (BCRP)
K_i (µM)	2.000
Organ/Tissue	Liver
Transporter	SLCO1B1 (OATP1B1)
K_i (µM)	0.067
Transporter	SLCO1B3 (OATP1B3)
K_i (µM)	0.070
Transporter	SLCO2B1 (OATP2B1)
K_i (µM)	11.400
Transporter	ABCB1 (P-gp/MDR1)
K_i (µM)	23.800
Transporter	ABCG2 (BCRP)
K_i (µM)	2.000
$f_{u,mic}$	1.000
Transport	
Active transport Papp-to-Peff correlation	Predicted
Active transport Papp-to-Peff correlation Slope	0.939
Active transport Papp-to-Peff correlation Intercept	-0.879
Organ/Tissue	Liver
Model	PerL
CL_{PD}(mL/min/10^6 cells)	1.00E-05
fuIW Type	User
fuIW	0.044
fuEW Type	Predicted
fuEW	1.000
Drug concentration for passive permeability	Unbound (ionised and unionised)
Transporter	SLCO1B1 (OATP1B1)
Location	Sinusoidal
Function	Influx
J_{max} (pmol/min/pmol Transporter)	4.000
K_m (µM)	0.500
f_{uinc}	1.000
ISEF,T	1.000

16 B/P, blood-to-plasma partition ratio; f_u, unbound drug fraction in plasma; f_a, absorption fraction; k_a, absorption
17 constant; f_u Gut, unbound drug fraction in gut lumen; Peff,man, in vivo human intestinal permeability; PCaco-2,

apparent permeability measured in Caco-2 model; V_{ss}, distribution volume at steady state; K_p, tissue-to-plasma partition coefficients; HLM CL_{int}, intrinsic clearance measured in human liver microsomal system; Biliary CL_{int} (Hep), intrinsic biliary clearance measured in SCHH system; CL_{renal}, renal excretory clearance; K_i, inhibition constant; $f_{u,mic}$, unbound drug fraction in microsomal system; CL_{PD}, passive diffusion clearance ; fuIW, unbound drug fraction in intracellular water; fuEW, unbound drug fraction in extracellular water; f_{uinc}, unbound drug fraction in in-vitro incubation system; K_m, Michaelis-Menten constant; J_{max}, in vitro maximum rate of transporter mediate uptake or efflux; ISEF,T, intersystem extrapolation factor for transporter study